Ann. Inst. H. Poincaré D
Comb. Phys. Interact. 11 (2024), 453–502
DOI 10.4171/AIHPD/167

Trisections in colored tensor models

Riccardo Martini and Reiko Toriumi

Abstract. We give a procedure to construct trisections for closed manifolds generated by colored tensor models without restrictions on the number of simplices in the triangulation, therefore generalizing previous works in the context of crystallizations and PL-manifolds. We give a description of how trisection diagrams can arise from colored tensor model graphs for closed 4-manifolds. We further speculate on generalization of similar constructions for a class of singular-manifolds generated by simplicial colored tensor models.

Contents

1. Introduction

One of the most remarkable results in theoretical physics lies in random matrix models [36] whose critical limit by 't Hooft's topological expansion [105] provides a universal random geometry as a Brownian map [80, 81, 86], which is proven [87–89] equivalent to Liouville continuum gravity (quantum gravity with dilaton field in two dimensions) [33, 95]. Upon introduction of non-trivial dynamics, matrix models can be shown to be mathematically rich. The theories based on Kontsevich-type matrix models [48, 70] can be reformulated as a non-commutative quantum field theory [49, 99, 100, 107], namely, the Grosse–Wulkenhaar model. The Grosse–Wulkenhaar mode

2020 Mathematics Subject Classification. Primary 81Q30; Secondary 81T32, 05E45.
Keywords. Trisections, tensor models, discrete topology, PL, piecewise linear topology, graph theory, colored graphs, graph encoding manifolds.

is an appealing quantum field theory with mathematical rigor, and exhibits properties like constructive renormalizability, asymptotic safety [37], integrability [46, 50], and Osterwalder–Schrader positivity [47, 51].

Tensor models are higher rank analogues of such random matrix models, which therefore lend themselves well to be a candidate to produce even more remarkable results for higher-dimensional random geometry and quantum gravity [34, 35, 59, 61, 97, 98]. Colored tensor models [64] in particular, are shown to represent fluctuating piecewise-linear (PL) pseudo-manifolds via their perturbative expansion in Feynman graphs encoding topological spaces [2]. Colored tensor models admit a $1/N$ expansion of the partition function [53, 54, 57] with a resummable leading order, given by melonic graphs [20], exhibiting critical behavior and a continuum limit [20]. Melonic graph amplitudes satisfy a Lie algebra encoded in the large N limit of the Schwinger–Dyson equations for tensor models [56]. Non-perturbative aspects such as Borel summability [58, 63, 66] and topological recursion [17, 19] are also studied.

Tensor models also provide a very interesting platform to explore new types of quantum/statistical field theory, owing to their non-local interactions and their vast combinatorics. As with matrix models, the combinatorial nature of tensor models can be enriched by introducing differential operators such that the resulting theory contains non-trivial dynamics. Consequently, the statistical model acquires a notion of scale and its $1/N$ expansion can be translated into a renormalization group flow of the theory. A series of analyses and results to understand the renormalization group flow can be found in the works [4, 5, 11, 22, 23, 25–27]. Different methods have been developed to accommodate the non-local nature of tensor models coming from combinatorics, such as dimensional regularization [12] and $4-\varepsilon$ expansion [24]. Having a formulation of renormalization group flow, one can then search for non-trivial fixed points, e.g., via functional renormalization group [6, 7, 9, 10, 14, 38, 77] and check their stability via Ward–Takahashi identities [78, 79]. Other non-perturbative studies include Polchinski equations [71, 72]. Moreover, in recent years, tensor models have found a new avenue of research in holography via the large N melonic limit, which is shared with the Sachdev–Kitaev–Ye model [60, 108]. Indeed, tensor models are a conceptually and computationally powerful tool not only to address random geometric problems but also problems in holography [31, 62, 68, 69, 73–75, 92–94], non-local quantum and statistical field theories, artificial intelligence [76], turbulence [32], linguistics [67, 96], and condensed matter [21], and serve as a very rich playground for theoretical physicists and mathematicians alike.

In the present work, we focus on studying the topological information encoded in the graphs generated by rank-4 colored tensor models. Understanding and revealing topological information and structure of PL-manifolds generated by tensor models are important work in the context of random geometry and quantum gravity. Of course, the present work is not the first one nor the only one to address the topological proper-

ties encoded in the PL-pseudo-manifolds that colored tensor models represent. In fact, there are precedent works examining topological spaces of tensor models [52, 55, 61, 64], e.g., homology and homotopy of the graphs have been presented. For three-dimensions, therefore correspondingly for rank-3 colored tensor models, Heegaard splitting has been identified in [103].

However, this particular work of ours focuses on a novel concept, trisections in four-dimensional topology, recently introduced by Gay and Kirby in 2012 [45]. Trisections are a novel tool to describe four-dimensional, closed, smooth manifolds by revealing the nested structure of lower-dimensional submanifolds. In particular, the trisection genus of a 4-manifold is an invariant of the DIFF category.[1] In the context of discrete manifolds, the trisection of all standard simply connected PL 4-manifolds has been studied for example in [3], and trisections in so-called crystallization graphs have been investigated in [29]. In the former work [3], they rely on Pachner moves to ensure that these submanifolds are handlebodies. However, in colored tensor models, we do not have the privilege to perform Pachner moves, since they are not compatible with colors in rank-4 tensor models. In the latter work [29], the study focused on crystallization graphs, which are very special graphs that ensure the connectivity of each of the submanifolds. However, in tensor models we generate also graphs which are not crystallizations, and furthermore, in the continuum limit of tensor models, where we are interested in large volume and refined triangulations, we will not find crystallization graphs dominating. Hence, crystallizations have a limited applicability in tensor models.

Therefore, we would like to address and formulate trisection in the colored tensor model setting in this work.

The paper is organized as follows. In Section 2, we review some key points related to colored tensor models, which our work is based on. In particular, in Section 2.1, we review the construction of tensor models and the definition of their partition function. In Section 2.2, we recall how Feynman graphs of colored tensor models can encode manifolds and what kind of topological information they store. In Section 3, we illustrate a few key concepts of three-dimensional topology necessary to our work. In Section 3.1, we explain how to describe manifolds via their handle decomposition and recall how, in the case of 3-manifolds, it encodes their Heegaard splitting. Section 3.2 analyzes the behavior of Heegaard splittings under connected sum, which will be of great importance in the later part of the paper, while in Sections 3.3 and 3.4, we review two constructions of Heegaard surfaces that are known in the literature and are based on combinatorial methods. Section 4, finally, is dedicated to the construction of trisections. After introducing the concept of trisection for smooth 4-manifolds, in

[1] Since in four dimensions DIFF $\sim$ PL, the trisection genus is also a PL-invariant.

Section 4.1 we review a particular kind of move, known as stabilization, and highlight some features that stabilization shares with connected sum of trisections. In Section 4.2, we focus on how to partition the vertices of a 4-simplex in three sets, which is the starting point of our construction of trisections. In Section 4.3, we study the structure obtained in a PL-manifold via our combinatorial construction and point out what kind of problems are encountered for a generic graph of a four-dimensional manifold. From this point onward, our work departs from previous results studying trisections via triangulations of 4-manifolds. In Section 4.4, finally, we show how the information about trisection can be extracted from the colored graph of rank-4 colored tensor models. Sections 4.5 and 4.6 elaborate on the analyses of the results. In particular, we prove that, indeed, we split the manifold under investigation into three four-dimensional handlebodies and we analyze the diagram generated by our procedure. Strictly speaking, this diagram gives rise to a collection of trisection diagrams of a given genus, as it is characterized by a redundant amount of attaching curves. Section 4.6 discusses such redundancy and explains how trisection diagrams can be obtained upon knowing the homotopy group of the central surface. It is worth mentioning here that all the trisection diagrams in such a collection are related by construction by a finite sequence of handle slides and stabilizations (examples are given in Appendix A). Section 4.7 addresses relaxation of the hypothesis of graphs dual to manifolds and illustrates in some cases that it is possible to draw a few topological conclusions for a wider class of graphs. Finally, in Section 5, we summarize our results and point out a few possible future directions which may benefit from the present work.

2. Tensor models

2.1. $(d+1)$-colored tensor models

In this section, we introduce tensor models, and in particular colored tensor models and some of their relevant objects which will be used later in order to construct trisections.

Tensor models are statistical theories of random tensors and can be thought of as zero-dimensional field theories. Then tensor models mostly encode combinatorial information and many of their properties can be directly imported to their higher-dimensional counterpart: tensor field theories. Colors are introduced via an extra index labeling the tensor themselves and we require the covariance of the theory to be diagonal with respect to the color indices. This last requirement will allow us to have a much greater control on the combinatorics encoded in the theory.

Besides the field content of the theory (e.g., rank of tensors and amount of colors considered), a colored tensor model is defined in perturbation theory upon specifying a free covariance and an array of interactions (deformations around the free theory). In this paper, we restrict to a simplicial model (the meaning of this name will be clear soon). We therefore consider the multiplicative group of integers modulo N, $\mathbb{Z}_N$ and let I be $\mathbb{Z}_N^{\times d}$ with elements $\mathbf{n} \in I$, $\mathbf{n} = \{n_1, \dots, n_d\}$ and $F(I)$ the space of complex functions on I. We give the following definition.

Definition 2.1. A $(d+1)$-colored tensor model of rank d tensors is defined via a measure $\mathrm{d}\nu$

$$\mathrm{d}\nu = \prod_{i=0}^{d} \mathrm{d}\mu_{C^i}(\phi^i, \bar{\phi}^i) e^{-S},$$

$$S = \lambda \sum_{\mathbf{n}_i \in I} \mathcal{K}_{\mathbf{n}_0 \cdots \mathbf{n}_d} \prod_{i=0}^{d} \phi^i_{\mathbf{n}_i} + \bar{\lambda} \sum_{\bar{\mathbf{n}}_i \in I} \bar{\mathcal{K}}_{\bar{\mathbf{n}}_0 \cdots \bar{\mathbf{n}}_d} \prod_{i=0}^{d} \bar{\phi}^i_{\bar{\mathbf{n}}_i},$$

where

- $\phi^i \colon I \to \mathbb{C}$ are $d+1$ complex random fields;
- $C^i \colon F(I) \to F(I)$ are $d+1$ covariances;
- $\mathcal{K}, \bar{\mathcal{K}} \colon I^{\times(d+1)} \to \mathbb{C}$ are two vertex kernels.

If $\mathcal{K}$ and $\bar{\mathcal{K}}$ are such that every tensor has exactly one index (n_i) contracted with another tensor in the interaction, we call the model a *simplicial* colored tensor model. Note that in the interaction term, every color index appears on the same footing, while the free measure factorizes in the product of single color measures. Thanks to this structure, the Feynman diagrams of a simplicial colored tensor model can be represented as *c*olored graph, i.e., a connected bipartite regular graph such that each line has a color in $\{0, 1, \dots, d\}$ and each node is incident to exactly one line of each color.[2]

Definition 2.2. A closed $(d+1)$-colored graph is a graph $\mathcal{G} = (\mathcal{V}, \mathcal{E})$ with node set $\mathcal{V}$ and line set $\mathcal{E}$ such that

- $\mathcal{V}$ is bipartite; there is a partition of the node set $\mathcal{V} = V \cup \bar{V}$, such that for any element $l \in \mathcal{E}$, $l = \{v, \bar{v}\}$, where $v \in V$ and $\bar{v} \in \bar{V}$. The cardinalities satisfy $|\mathcal{V}| = 2|V| = 2|\bar{V}|$.

[2] In the following, we will often have to go back and forth between graphs and triangulation. Therefore, in order to avoid confusion, we will adopt the terms *node* and *line* for, respectively, zero-dimensional and one-dimensional objects in a graph, while we will call *vertex* and *edge* a zero-dimensional and a one-dimensional object in the triangulation. When referring to edges on the boundary of two-dimensional polygons we might use the term *sides*.

- The line set is partitioned into $d+1$ subsets $\mathcal{E} = \bigcup_{i=0}^{d} \mathcal{E}^i$, where $\mathcal{E}^i$ is the subset of lines with color i.
- It is $(d+1)$-regular (i.e., all nodes are $(d+1)$-valent) with all lines incident to a given node having distinct colors.

To distinguish, we call the elements $v \in V$ ($\overline{v} \in \overline{V}$) positive (negative) nodes and draw them with the colors clockwise (anti-clockwise) turning. We often denote by these positive (negative) nodes in colors black (white) in graphs. The bipartition also induces an orientation on the lines, say from v to $\overline{v}$.

We notice that $(d+1)$-colored graphs are dual to (colored) simplicial triangulations of piecewise linear (PL) orientable pseudo-manifolds[3] in d dimensions [2, 43, 52]. In particular, every node in the graph corresponds to a top-dimensional simplex, every line is dual to a $(d-1)$-dimensional face and two nodes joined by a line of color i represent a pair of d-simplices sharing the same $(d-1)$-face (i.e., an orientation reversing homeomorphism between the two boundary faces is implied). In fact, given a simplicial colored triangulation $\mathcal{T}$ of a PL pseudo-manifold M, one can consider the dual cellular decomposition $\mathcal{T}^*$ and notice that a colored graph is nothing but the 1-skeleton of $\mathcal{T}^*$. Therefore, colored graphs are often referred to as *graph encoding manifolds* (GEM), and play a fundamental role in the study of PL topological invariant from a combinatorial point of view, especially within the framework of crystallizations [43]. We remark that not every triangulation can be colored, although a refinement compatible with edge coloring can always be found by means of barycentric subdivision.

We postpone a more detailed explanation of the topological description of colored graphs to the following sections. Nevertheless, it is useful to recall here how to embed a colored graphs in its dual triangulation. Consider a triangulation $\mathcal{T}$ of a 4-manifold M, and a colored graph $\mathcal{G}$ dual to $\mathcal{T}$, therefore $K(\mathcal{G}) = \mathcal{T}$ and $|K(\mathcal{G})| = M$. The most natural prescription is to embed the graph such that every component of the graph intersects its dual simplex transversally and at the barycenter. Since the graph is the 1-skeleton of the dual cellular decomposition of M, it is only made of nodes and lines. Therefore, we only have to embed nodes in the barycenter of d-simplices and have i-colored lines intersecting i-colored $(d-1)$-faces transversally. Examples are shown in Figure 1. For example in four dimensions we will have nodes at the center of 4-simplices and i-colored lines intersecting i-colored tetrahedra transversally. Although very simple, this embedding represents a very powerful tool to understand many topological properties of PL manifolds using colored graphs.

[3] A pseudo-manifold is characterized by being non-branching, strongly-connected, and pure to ensure a rather nice property for a d-dimensional simplicial complex. However, $K(\mathcal{B}^{\hat{i}})$ may not represent a manifold, i.e., $K(\mathcal{B}^{\widehat{ij}})$ may not be a sphere [52].

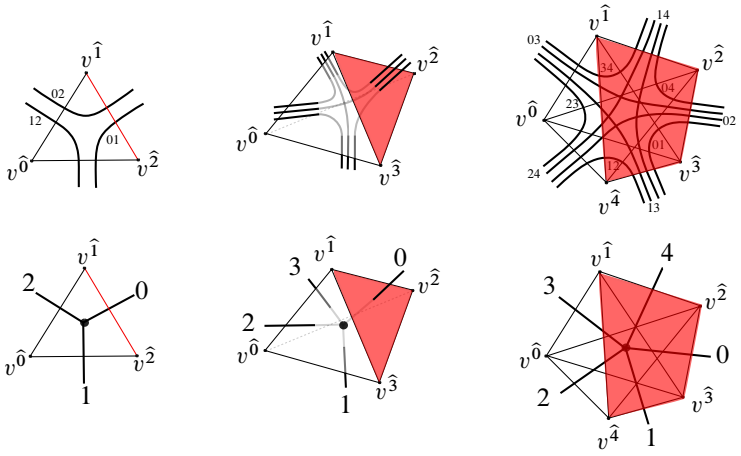

Figure 1. We show d-simplices in dimensions $d = 2, 3, 4$, where we also embedded $(d + 1)$-colored graphs. From left to right, $d = 2, 3, 4$, and on the top row, embedded tensor model graphs are shown in stranded representation, and on the bottom row, shown in colored representation. We show in red, 0-colored faces (one-dimensional for rank 2, two-dimensional for rank 3, and three-dimensional for rank 4).

As a final remark, we point out that bipartiteness of a colored graphs $\mathcal{G}$, which from a tensor model point of view follows from employing complex tensors and a real free covariance, implies orientability of $K(\mathcal{G})$ [2]. Both in the GEM formalism and in tensor models, this condition can be relaxed if non-orientable (pseudo-)manifolds shall be considered, nevertheless, in this paper we restrict ourselves to the orientable case.

2.2. Topology of colored graphs

As advertised, these colored graphs are extensively studied in topology especially in the form of crystallization [30, 42, 82]. One can say that the colors therefore are responsible to encode enough topological information to construct a d-dimensional cellular complex, rather than the a priori naive 1-complex of a graph. Most of the topological information is encoded within different kinds of embedded sub-complexes of $K(\mathcal{G})$ and their combinatorial description in terms of colored graphs.

Bubbles. The first structure we present is that of *bubbles*.[4] Starting from a colored graph $\mathcal{G}$ dual to a colored triangulation $\mathcal{T} = K(\mathcal{G})$, a n-bubble $\mathcal{B}_a^{i_1,\dots,i_n}$ is the a-th connected component of the subgraph spanned by the colors $i_1, \dots, i_n \in \{0, \dots, d\}$.

[4] Sometimes referred to as *residues* in the literature.

In order to lighten the notation, we will indicate d-bubbles by their only lacking color and sometimes we will refer to them as $\hat{i}$-bubble, for example in four dimensions we might consider the $\hat{0}$-bubble $\mathcal{B}_a^{\hat{0}} = \mathcal{B}_a^{1,2,3,4}$. Each bubble identifies a single simplex in $\mathcal{T}$, in particular given a n-bubble $\mathcal{B}_a^{i_1,\ldots,i_n}$, its dual $K(\mathcal{B}_a^{i_1,\ldots,i_n})$ is PL-homeomorphic to the link of a $(d-n)$-simplex σ_a in the first barycentric subdivision of $\mathcal{T}$. Upon the embedding procedure described above, we can think about $K(\mathcal{B}_a^{i_1,\ldots,i_n})$ as the boundary of a n-dimensional submanifold of $\mathcal{T}$, intersecting σ_a transversally. The most important bubbles for our work are d-bubbles and 2-bubbles. d-bubbles represent the link of vertices (0-simplices) in $\mathcal{T}$. A standard result states that $K(\mathcal{G})$ is a manifold if and only if all d-bubbles are topological spheres. 2-bubbles will be referred to as bicolored cycles,[5] they identify $(d-2)$-simplices (triangles in four dimensions) and are often depicted in tensor models when employing the "stranded" notation for Feynman graphs. From a tensor model perspective, while nodes of $\mathcal{G}$ correspond to interaction vertices and lines to free propagators of the theory, bicolored cycles come from the contraction patterns of tensor indices.

Jackets. Let $\mathcal{G}$ be a $(d+1)$-colored graph. For any cyclic permutation $\eta = \{\eta_0, \ldots, \eta_d\}$ of the color set, up to inverse, there exist a regular cellular embedding of $\mathcal{G}$ into an orientable surface Σ_η, such that regions of Σ_η are bounded by bicolored cycles labeled by $\{\eta_i, \eta_{i+1}\}$ [8,53,54,57]. Then, we define a jacket $\mathcal{J}_\eta$ as the colored graph having the same nodes and lines as $\mathcal{G}$, but only the bicolored cycles $\{\eta_i, \eta_{i+1}\}$.

Definition 2.3. A colored *j*acket $\mathcal{J}_\eta$ is a 2-subcomplex of $\mathcal{G}$, labeled by a permutation η of the set $\{0, \ldots, d\}$, such that

- $\mathcal{J}_\eta$ and $\mathcal{G}$ have identical node sets, $\mathcal{V}_\mathcal{J} = \mathcal{V}_\mathcal{G}$;
- $\mathcal{J}_\eta$ and $\mathcal{G}$ have identical line sets, $\mathcal{E}_\mathcal{J} = \mathcal{E}_\mathcal{G}$;
- the bicolored cycle set of $\mathcal{J}_\eta$ is a subset of the bicolor set of $\mathcal{G}$: $\mathcal{F}_\mathcal{J} = \{f \in \mathcal{F}_\mathcal{G} | \ f = \{\eta_i, \eta_{i+1}\}, i \in \mathbb{Z}_{d+1}\}$.

From a tensor model perspective, jackets are merely ribbon graphs (only comprise of nodes, lines and bicolored cycles), like the ones generated by matrix models graphs. See examples of jackets in Figure 2. Therefore, jackets represent embedded surfaces in the cellular complex represented by colored tensor models graphs. Let us clarify this point. The regular embedding of $\mathcal{G}$ into Σ_η defines a cellular decomposition of Σ_η with polygonal 2-cells having $(d+1)$-sides. Each 2-cell is dual (in Σ_η) to a node of $\mathcal{G}$ and each side is dual to a line (furthermore, every vertex is dual to a bicolored cycle $\{\eta_i, \eta_{i+1}\}$). Therefore, sides inherit the colors carried by lines of $\mathcal{G}$. One may

[5] In the tensor models literature, we often refer to bicolored cycles as faces, however, in this paper, we will keep the word faces for general simplices.

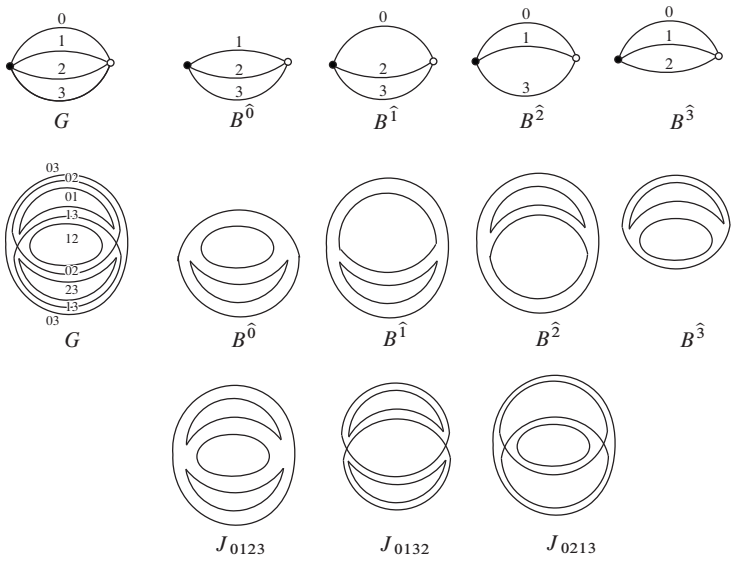

Figure 2. We show in the top row the colored representations of the elementary melon $\mathcal{G}$ in rank-3 tensor bipartite colored model, its bubbles $\mathcal{B}^{\hat{0}}$, $\mathcal{B}^{\hat{1}}$, $\mathcal{B}^{\hat{2}}$, and $\mathcal{B}^{\hat{3}}$ from left to right. In the middle row, we show the stranded representations of the same objects as the top row. In the bottom row, we show in the stranded representation, the jackets of the elementary melon in rank 3 tensor bipartite colored model.

notice that the transversal intersection of a surface with a codimension-1 i-simplex is a one-dimensional edge homeomorphic to such an i-colored side. Therefore, we can think that $K(\mathcal{J}_\eta)$ is an embedding of Σ_η in $K(\mathcal{G})$, such that it intersects transversally all the $(d-1)$-faces. If $d < 3$, the dimensionality of Σ_η is too low to define two different regions within the top-dimensional simplices. If $d = 3$, however Σ_η splits every top-dimensional simplex and have been shown to represent Heegaard surfaces of three-dimensional PL-manifold $K(\mathcal{G})$ [103]; we discuss this further in Section 3.3.

It is evident that $\mathcal{J}$ and $\mathcal{G}$ have the same connectivity. We note here that the number of independent jackets is $d!/2$. We define the *Euler characteristic* of the jackets as $\chi(\mathcal{J}) = 2 - 2g_{\mathcal{J}} = |\mathcal{V}_{\mathcal{J}}| - |\mathcal{E}_{\mathcal{J}}| + |\mathcal{F}_{\mathcal{J}}|$, where $g_{\mathcal{J}}$ is the genus of the jacket and corresponds to the genus of Σ_η. Note that we only define jackets for the closed colored graphs here. We also remark that jackets are also bipartite reflecting the definition above, and therefore represent orientable surfaces.

Gurau degree. From a tensor model perspective, jackets play a crucial role in the large N expansion of colored tensor models, as they define the so-called Gurau degree, which is the parameter that governs the large N expansion. For completeness, we introduce the Gurau degree of a graph $\mathcal{G}$ as follows.

Definition 2.4. Given colored graph $\mathcal{G}$ and the set of its jackets, we define a combinatorial invariant, called *Gurau degree*, as the sum of genera of all jackets of $\mathcal{G}$: $\omega(\mathcal{G}) = \sum_{\mathcal{J}} g_{\mathcal{J}}$. It is easy to see that ω is a non-negative integer.

A remarkable feature of Gurau degree is that if $\omega = 0$, then the $K(\mathcal{G})$ is a topological sphere, although the converse is not always true. Although for $d = 2$ the degree equals the genus of the triangulation dual to $\mathcal{G}$, it is not a topological invariant for $d > 2$. However, it is an important quantity in tensor models, as the classification of graphs organized by the Gurau degree allows for a $1/N$ expansion where N is the size of the tensors, just like the $1/N$ expansion of matrix models according to the genus. We refer to other literature [53, 54, 57] for a more detailed discussion on the large N expansion of colored tensor models.

3. Heegaard splittings of 3-manifolds

In this section, we introduce some of the concepts that are pedagogical to understanding trisections and to which we refer often in later sections of the paper, namely handle decomposition and Heegaard splittings. We begin defining such constructions for objects in the TOP category (specifically for three-dimensional topological manifolds in the case of Heegaard splittings), and we restrict later to the PL category, which is the main focus of this work.

3.1. Attaching handles

A handle decomposition of a closed and connected topological d-manifold M is a prescription for the construction of M by subsequently attaching handles of higher index. We can define an i-handle in d dimensions as a topological d-ball D^d parametrized as $\mathrm{D}^i \times \mathrm{D}^{d-i}$ and is glued to a manifold K along $\mathrm{S}^{i-1} \times \mathrm{D}^{d-i}$, i.e., there exist an orientation reversing homeomorphism from $\mathrm{S}^{i-1} \times \mathrm{D}^{d-i}$ to a subset of ∂K. Therefore, an i-handle can be viewed as the thickening of an i-dimensional ball (which we call *spine*); we will refer to the boundary of this ball as the *attaching sphere* of the handle. A $(d-i)$-ball intersecting the spine transversally, is called compression disc, and its intersection with the boundary of the handle is referred to as *belt sphere*. Note that, unless the handle decomposition of a manifold includes at least one top-dimensional handle, the result always has a boundary. See Figure 3 for the illustration of anatomy of handles.

Definition 3.1. A *handlebody* H (sometimes referred to as 1-*handlebody*) is a manifold whose handle decomposition contains only a 0-handle and 1-handles. The genus g of H can be defined as the number of 1-handles in its decomposition.

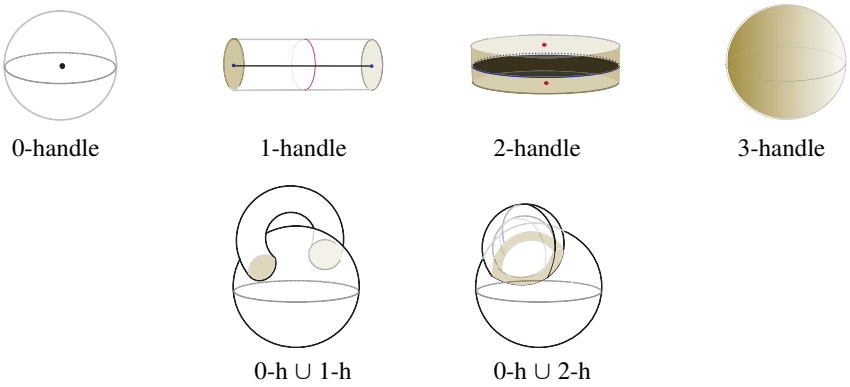

Figure 3. Handles in three dimensions. The figure shows (from left to right) a three-dimensional a 0-handle (D^3), a 1-handle ($D^1 \times D^2$ glued along $S^0 \times D^2$), a 2-handle ($D^2 \times D^1$ glued along $S^1 \times D^1$), and a 3-handle (D^3 glued along S^2). The gluing surfaces are colored in brown. For 0-handle, the spine is a point, for 1-handle the spine is a line, and for 2-handle the spine is a disc, all colored in solid black. We also show in red belt spheres for 1-handle and 2-handle. Lastly, we also illustrate how 1-handles and 2-handles attach to a 0-handle at the gluing region which are colored in brown.

Note that, if H is three-dimensional, then g equates the genus of ∂H. Moreover, a manifold is a handlebody if and only if it collapses to a one-dimensional spine.

Definition 3.2. Let H_1 and H_2 be two three-dimensional handlebodies of genus g and let f be an orientation reversing homeomorphism from ∂H_1 to ∂H_2. We call (H_1, H_2, f) a *Heegaard splitting* of the 3-manifold M if

$$M = H_1 \bigcup_f H_2. \tag{3.1}$$

The common boundary $\Sigma = \partial H_1 = \partial H_2$ is then called a *Heegaard surface*.

From now on, making use of a slight abuse of notation and for the sake of clarity, we represent a Heegaard splitting with the triple $M = (H_1, H_2, \Sigma)$, by asserting $\Sigma = \partial H_1 = \partial H_2$ is provided by the homeomorphism f.

A Heegaard splitting allows us to represent a closed and compact 3-manifold[6] M via a surface and two sets of closed lines on the surface representing the homotopically

[6]In the present manuscript, we focus on closed and orientable manifolds, nevertheless the definition of Heegaard splitting applies to a wider class of manifolds. In particular, we point out that in the case of non-orientable 3-manifold, the Heegaard surface is non-orientable as well [101]. Moreover, the definition of Heegaard splitting can be extended to manifold with boundary making use of compression bodies instead of handlebodies [85].

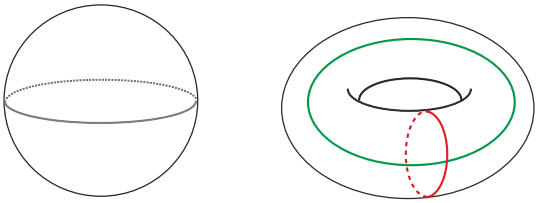

Figure 4. Heegaard diagrams for S^3. The picture shows two Heegaard diagrams (out of infinitely many with arbitrary genus g) for the sphere S^3: for minimum genus $g = 0$ (on the left), and for $g = 1$ (on the right). The diagram with a Heegaard surface $g = 0$ (S^2) does not have any attaching curves. The α- and β-curves on the Heegaard surface $g = 1$ ($S^1 \times S^1$)are shown in red and blue. The toric Heegaard surface in the latter is the common boundary of two solid tori ($D^2 \times S^1$): we can consider them so that inside this toric Heegaard surface, there is one solid torus, and there is another one outside. In particular, we can consider the diagram as embedded in $\mathbb{R}^3$ plus a point at infinity (therefore in a space homeomorphic to S^3). The outside solid torus is specified by the blue β-curve which is the boundary of a horizontally lying compression disc. Its spine would circle around the torus intersecting this compression disc transversally. Note that if one views the blue curve as the attaching sphere of a 2-handle, the resulting manifold would be a topological ball D^3, which can be easily capped-off to generate S^3.

inequivalent belt spheres of each handlebody. These curves, namely α- and β-curves, encode the information on how H_1 and H_2 are glued to their boundaries. We refer to α- and β- curves collectively as *attaching curves*.

The representation we just described is called a *Heegaard diagram* for M. Figure 4 shows two examples of Heegaard diagrams for the 3-sphere. It is important to point out that cutting Σ along the α-curves or along the β-curves never leads to a disconnected surface, instead we obtain a 2-sphere from which an even number of discs (two per each curve) have been removed. See Figure 5.

We should point out the symmetry between i-handles and $(d - i)$-handles in d dimensions. Since $\partial(D^i \times D^{d-i}) = (S^{i-1} \times D^{d-i}) \cup (D^i \times S^{d-i-1})$, the difference between the two types of handles is which portion of the handle's boundary is glued onto a manifold and which part remains for other handles to be glued on. In particular, the 1-handles and 3-handles of H_2 in (3.1), glue onto H_1 as 2-handles and 3-handles, respectively.

Finally, we point out that a Heegaard splitting of a 3-manifold is not unique, nevertheless two splittings of the same manifold (and the respective Heegaard diagrams), are always connected by a finite sequence of moves, called *Heegaard moves*, consisting in:

- handle slides,
- insertion/removal of topologically trivial couples of 1-handle and 2-handle (i.e., glued in such a way that together they form a 3-ball D^3).

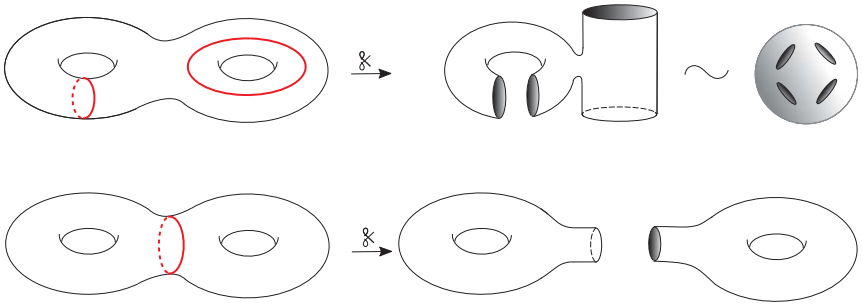

Figure 5. Cutting along attaching curves. An example of viable attaching curves (top) and a not viable one (bottom). Note that cutting along the latter separated the would-be Heegaard surface in two connected components.

Definition 3.3. Given a 3-manifold M, the minimal genus over all the possible Heegaard surfaces is a topological invariant. We call this number *Heegaard genus*.

3.2. Connected sum and Heegaard splittings

The *connected sum* $M \sharp N$ of two d-manifolds M and N is constructed by removing a topological d-ball D^d from their interior and gluing M and N by identifying their boundaries (homeomorphic to S^{d-1}). If M and N are both oriented, there is a unique connected sum constructed through an orientation reversing map between the boundaries after the removal of the d-balls and the resulting manifold is unique up to homeomorphisms.

We define the *boundary-connected sum* of two d-manifolds with boundaries, M and N, as the manifold $M \natural N$ obtained by performing a connected sum of their boundaries $\partial M \sharp \partial N$. Note that the boundary-connected sum of handlebodies H_1 and H_2 is a handlebody itself. The spine of $H_1 \natural H_2$ can be represented by joining the two spines through a line or a point.[7]

A question that naturally arises is: given two 3-manifolds M and N, is there a way to represent a Heegaard splitting of $M \sharp N$ in terms of Heegaard splittings $M = \{H_1, H_2, \Sigma_M\}$ and $N = \{K_1, K_2, \Sigma_N\}$? To answer this question, we consider a 3-ball D_M (resp. D_N) intersecting Σ_M (Σ_N) transversally in one 2-ball. Since the result is unique up to homeomorphism, we can choose the ball to be removed as better

[7] The line connecting the two spines does not represent any handle, rather, the identification of two discs on the boundaries of the two handlebodies and, therefore, can be contracted to a point. Nevertheless, it is useful for the moment to consider it as a specification of the way the boundary-connected sum is performed.

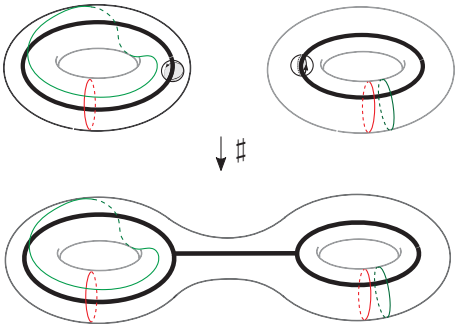

Figure 6. Connected sum. We represent here the connected sum of 3-manifolds via their Heegaard diagrams (Lens space $l(1,1)$ on the left, $S^1 \times S^2$ on the right). The picture shows the balls to be removed (castration) from the manifolds and how they intersect the Heegaard surfaces. Note that this corresponds to the boundary-connected sum of the handlebodies. We show in the solid black thick line as the spine of the handlebodies, and the attaching curves are in red and in green. The arrows along the circles on the Heegaard surface show the reversed orientation.

suits us. Since the intersection of the 3-ball with each element of the splittings is a ball of the appropriate dimension, the connected sum of $M \sharp N$ performed removing D_M and D_N naturally gives rise to a Heegaard splitting of the form $\{H_1 \natural K_1, H_2 \natural K_2, \Sigma_M \sharp \Sigma_N\}$. See Figure 6 for an explicit example.

A few comments are in order. Firstly, we remark that the Heegaard splitting of closed manifolds is symmetric with respect to the two handlebodies. By this we mean that we can differentiate H_1 and H_2 through labels induced by the construction of the splitting, but ultimately their role (and therefore the role of α-curves and β-curves) can be interchanged. For example, if we have in mind a handle decomposition of M we can say that H_1 is given by the set of handles of index $i \leq 1$ while H_2 is given by the set of handles with $i \geq 2$ but, as we explained above, these characterizations can be easily switched for three-dimensional manifolds upon inverting the gluing order of the handles. If we induce the Heegaard splitting via a self-indexing Morse function f via $f^{-1}(3/2)$, the role of the handlebodies can be switched upon sending f to $-f+3$. In agreement with this feature of Heegaard splittings, we notice that H_1 and H_2 induce, as submanifolds of M, an opposite orientation of Σ_M. This might create an ambiguity in performing the connected sum $M \sharp N$ through the Heegaard splittings of M and N since reversing the orientation of one of the two Heegaard surfaces corresponds to a different boundary-connected sum of the handlebodies involved in the construction. This ambiguity reflects the fact that the connected sum is unique only after specifying the orientation of the manifolds involved.[8] Ultimately, a choice of α-

[8] An example of connected sum between three-dimensional manifolds in which reversing the orientation of one of the manifolds involved changes the result is $l(3,1) \sharp l(3,1)$, which is not

and β-curves for the two diagrams corresponds to a choice of relative orientation for the two manifolds and specifies a connected sum constructed so that the set of α-curves in $M \sharp N$ is the union of the sets of α-curves in M and α-curves in N and similarly for the β-curves.

Secondly, we point out that the choice of a disc to be removed from each Heegaard surface during the connected sum operation is irrelevant, provided it does not intersect any attaching curve. To convince oneself, it is sufficient to remember that cutting along all the α-curves we obtain a pinched sphere on which any discs are equivalent, and similarly for the β-curves.

3.3. Jackets as Heegaard surfaces

Turning our attention to objects in the PL category, in particular to PL 3-manifolds encoded in colored graphs, one might wonder whether there exists a natural formulation of Heegaard splittings in terms of combinatorial objects. In [103], it is shown that the Riemann surfaces corresponding to the jackets of a rank-3 colored tensor model are Heegaard surfaces, and that if the corresponding triangulation is a manifold, then the triple $(K(\mathcal{J}^{(ij,\widehat{ij})}), H^{(ij)}, H^{(\widehat{ij})})$ is a Heegaard splitting of the triangulation. Although the complex structure of the Riemann surfaces studied in [103] was merely a consequence of the field content of the model examined, the Heegaard structure is purely combinatorial. In fact, this identification was already known in the crystallization theory literature, and led to the formulation of the concept of regular genus [44]. Here, we revise such construction which will be of great importance in the following.

Let us consider a three-dimensional connected orientable closed manifold M dual to a rank-3 colored tensor model graph $\mathcal{G}$ which is introduced in Section 2: $M = K(\mathcal{G})$. For every 3-simplex $\Delta^{(3)} \in \mathcal{T}$, we consider a function f mapping $\Delta^{(3)}$ onto $[0, 1] \in \mathbb{R}$ as in Figure 7. We recall that in every $\Delta^{(3)}$, each edge is uniquely defined by a pair of colors $\{i, j\}$, where $i, j \in 0, 1, 2, 3$. We can construct f such that the preimage of the points $\{\{0\}, \{1\}\}$ under f identifies everywhere in $\mathcal{T}$ two non-intersecting edges of given colors $f^{-1}(0) = \{i, j\}$, $f^{-1}(1) = \{k, l\}$, $i, j, k, l \in \{0, 1, 2, 3\}$, $i \neq j \neq k \neq l$, while the preimage of any point in $(0, 1)$ gives us a square cross section of each $\Delta^{(3)}$. We can glue these squares via their boundaries according to the colors, obtaining a surface embedded in M. The surface Σ constructed in this way is a realization of a quadrangulation represented by one the jackets $\mathcal{J}_{\{i,j\}\{k,l\}}$ of $\mathcal{G}$ and is dual to the corresponding matrix model obtained by removing the strands

homeomorphic to $l(3, 1) \sharp \overline{l(3, 1)}$, where $\overline{l(3, 1)}$ represents $l(3, 1)$ with the opposite orientation. A similar feature happens in four dimensions with the two possible connected sums of $\mathbb{CP}^2$ with itself.

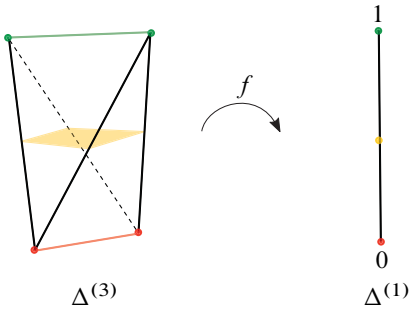

Figure 7. Mapping of a 3-simplex $\Delta^{(3)}$. f is a map from a d-simplex $\Delta^{(d)}$ to a $\lfloor \frac{d}{2} \rfloor$-simplex $\Delta^{\lfloor \frac{d}{2} \rfloor}$, $\lfloor x \rfloor$ being the floor function of x; here, it is for $d = 3$. As we will explain later, the 0-skeleton of the first barycentric subdivision of $\Delta^{\lfloor \frac{d}{2} \rfloor}$ minus the 0-skeleton of $\Delta^{\lfloor \frac{d}{2} \rfloor}$ itself defines the splitting and its preimage represents, in this case, a square in the Heegaard surface. The 0-skeleton of $\Delta^{\lfloor \frac{d}{2} \rfloor}$ defines the spines of the handlebodies. By linearly extending this identification, we can reconstruct the entire tetrahedron [102].

$\{i, j\}$ and $\{k, l\}$.[9] Since the graph $\mathcal{G}$ is closed, bipartite and connected, so is $\mathcal{J}$. The surface Σ therefore splits M in two manifolds H_0 and H_1 with their common boundary being the surface Σ itself. It is easy to notice that the spine of each H_i is one-dimensional. In fact, it is given by the set of edges $f^{-1}(i)$ for $i \in \{0, 1\}$. Thus, H_0 and H_1 are handlebodies and a jacket $\mathcal{J}$ identifies a Heegaard surface Σ.

Once we identified a Heegaard splitting of M in terms of combinatorial objects (i.e., via jackets) as described above, it is natural to wonder how the attaching curves arise. As we can see from Figure 8, for every edge e in the spine of H_i we can construct a compression disc in the shape of a polygon. The intersection of the compression disc with each of the tetrahedra sharing e is a triangle (Figure 8) and the disc is therefore a polygon whose sides are as many as the number of the 3-simplices sharing e. Importantly, we see that the perimeter of the polygon is the projection of the edges opposite to the spine on the Heegaard surface. This implies that, given the quadrangulation of Σ defined by a jacket $\mathcal{J}$, we can draw the attaching curves by connecting the opposite edges of each square.

A remark is in order. The construction of attaching curves drawn on a Heegaard surface we described so far is, in a way, overcomplete since it provides us with a redundant description; we will end up having many copies of the same curve (i.e., ho-

[9]Here we employ a slightly different notation for jackets with respect to the one introduced in Section 2.2. Notice that, if $d = 3$, the set of bicolored cycles in the jacket is lacking only two elements from the set of bicolored cycles of $\mathcal{G}$. Thus, by writing $\mathcal{J}_{\{i,j\}\{k,l\}}$ we mean that $\{i, j\} \notin \{\{\eta_i, \eta_{i+1}\} \forall i \in \mathbb{Z}_4\}$ and similarly for $\{k, l\}$. This notation is especially convenient in order to understand jackets in terms of Heegaard splittings.

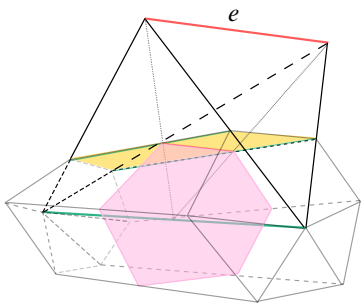

Figure 8. A compression disc, an attaching curve and a spine of three-dimensional handlebody. The central green line is a single edge in the triangulation, shared by six 3-simplices, which is to be identified as a spine of a three-dimensional handlebody. The rectangular faces (one of them colored in yellow) of the hexagonal prism are part of the Heegaard surface Σ. A compression disc is depicted in pink (a hexagon) and its intersection with the Heegaard surface is an attaching curve. As illustrated above, a segment of an attaching curve can be considered as a projection on Σ of the edge opposite to the spine (e) in each 3-simplex.

motopically equivalent ones) and furthermore, curves that are homotopic to a point (which hence should not be considered since they describe the attaching of a sphere). It is sufficient to consider only one representative of each equivalence class,[10] nevertheless, when constructing a trisection later on, a bit of care will be needed to convince ourselves that such freedom does not imply any ambiguity in the construction.

For completeness, we compute here the genus of the Heegaard surface obtained with the procedure described above. Since $\Sigma = K(\mathcal{J})$, we have that the genus g_Σ is given by

$$g_\Sigma = \frac{2-\chi_{\mathcal{J}}}{2} = \frac{1}{2}(2 - V_{\mathcal{J}} + E_{\mathcal{J}} - F_{\mathcal{J}}),$$

where $\chi_{\mathcal{J}}$ is the Euler characteristic of $K(\mathcal{J})$ and $V_{\mathcal{J}}$, $E_{\mathcal{J}}$ and $F_{\mathcal{J}}$ the vertices, edges and bicolored paths in $\mathcal{J}$, respectively. Since the vertices and the edges in the jacket are the same as those in $\mathcal{G}$, and they satisfy $2E_{\mathcal{G}} = 4V_{\mathcal{G}}$, we can further write

$$g_\Sigma = 1 + \frac{1}{2}V_{\mathcal{G}} - \frac{1}{2}F_{\mathcal{G}} \geq 0. \tag{3.2}$$

3.4. More Heegaard splittings in triangulable manifolds

For later convenience, we illustrate now a different construction of Heegaard splittings from which we will borrow its technique later on. Consider a triangulation $\mathcal{T}$

[10] We stress that an α-curve and a β-curve can be homotopically equivalent and that the operation of modding out the equivalence class should be performed in either set independently.

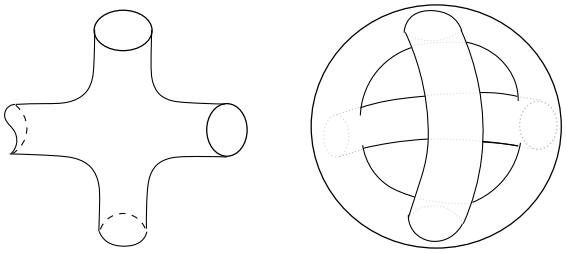

Figure 9. A schematic representation of the two handlebodies obtained for a single tetrahedron using the 1-skeletons of $\mathcal{T}$ and $\mathcal{T}^*$.

of a PL manifold M and its dual cellular decomposition $\mathcal{T}^*$. The 1-skeletons of $\mathcal{T}$ and $\mathcal{T}^*$ are perfect candidates to be identified as spines of H_1 and H_2. In fact, H_1 and H_2 are nothing but tubular neighborhoods of these two 1-skeletons, providing an orientation reversing homeomorphism between their boundaries, we can identify the Heegaard surface (see Figure 9). Note that if $\mathcal{T}$ is the triangulation associated with a colored graph $\mathcal{G}$, the 1-skeleton of $\mathcal{T}^*$ is the graph itself. The Heegaard genus g is then given by

$$g = E_{\mathcal{T}} - V_{\mathcal{T}} + 1 = E_{\mathcal{T}^*} - V_{\mathcal{T}^*} + 1 = V_{\mathcal{T}^*} + 1, \tag{3.3}$$

where $E_{\mathcal{T}}$ ($E_{\mathcal{T}^*}$) and $V_{\mathcal{T}}$ ($V_{\mathcal{T}^*}$) are the number of edges and vertices in the 1-skeletons of $\mathcal{T}$ ($\mathcal{T}^*$). The genus then corresponds to the number of independent loops of each graph, i.e., the dimension of the first homology groups of the 1-skeletons. Note that, by definition, $V_{\mathcal{T}^*}$ corresponds to the number of tetrahedra in $\mathcal{T}$, which we denote by $F_{\Delta^{(3)}_{\mathcal{T}}}$, while $E_{\mathcal{T}^*}$ is the number of triangles in $\mathcal{T}$, which we denote by $F_{\Delta^{(2)}_{\mathcal{T}}}$. Therefore, equation (3.3) leads to the following identity for the Euler characteristic of M:

$$\chi(M) = V_{\mathcal{T}} - E_{\mathcal{T}} + F_{\Delta^{(2)}_{\mathcal{T}}} - F_{\Delta^{(3)}_{\mathcal{T}}} = 0,$$

which is always true for odd-dimensional manifolds due to the Poincaré duality [91].

Finally, if we compare the present construction with the one obtained in Section 3.3 we can find from equation (3.2) (and using the fact that $\mathcal{G}$ is the 1-skeleton of $\mathcal{T}^*$):

$$g_\Sigma - g = -\frac{1}{2}(V_{\mathcal{T}^*} + F_{\mathcal{G}}) < 0.$$

Therefore, we notice that $g_\Sigma < g$, which imply that this way of constructing a Heegaard splitting is actually less advantageous, as the topological invariant is the minimum genus of Heegaard surface.

4. Trisections

A construction analogous to a Heegaard splitting (in three-dimensions) can be performed in four-dimensions, which is called *trisection* [45]. Note that one can perform trisections for non-orientable manifolds [104], however in this paper, we restrict ourselves to orientable manifolds. Again, we start by working within the TOP category. We will restrict to objects in the PL category later in the paper.

Definition 4.1. Let M be a closed, orientable, connected 4-manifold. A trisection of M is a collection of three submanifolds $X_1, X_2, X_3 \subset M$ such that:

- each X_i is a four-dimensional handlebody of genus g_i,
- the handlebodies have pairwise disjoint interiors $\partial X_i \supset (X_i \cap X_j) \subset \partial X_j$ and $M = \bigcup_i X_i$,
- the intersection of any two handlebodies $X_i \cap X_j = H_{ij}$ is a three-dimensional handlebody,
- the intersection of all the four-dimensional handlebodies $X_1 \cap X_2 \cap X_3$ is a closed connected surface Σ called *central surface*,

for $i, j \in 1, 2, 3$.

Note that any two of the three-dimensional handlebodies $\{H_{ij}, H_{jk}, \Sigma\}$ form a Heegaard splitting of ∂X_j.

In four dimensions, we have the following *extending theorem* [90]:

Theorem 4.2. *Given a four-dimensional handlebody H of genus g and an homeomorphism $\phi\colon \partial H \to \partial H$, there exists a unique homeomorphism $\Phi\colon H \to H$ which extends ϕ to the interior of H.*

It implies that closed 4-manifolds are determined by their handles of index $i \leq 2$ and that there is a unique cap-off determining the remaining 3- and 4-handles (recall the symmetric roles of i-handles and $(4-i)$-handles in four dimensions). However, in the context of trisections, the extending theorem plays an even bigger role, for it can be applied to each handlebody X_i in Definition 4.1. Consequently, a trisection of M is fully determined by the three three-dimensional handlebodies H_{ij} which, in turn, can be represented by means of Heegaard diagrams.

Hence, similarly to the three-dimensional case of Heegaard splittings, a trisection can be represented with a diagram consisting of the central surface[11] Σ and three sets

[11] From now on we may adopt the term "central surface" for both the case of trisections and Heegaard splittings when a feature is clearly common to the central surface of a trisection and the Heegaard surface of a Heegaard splitting.

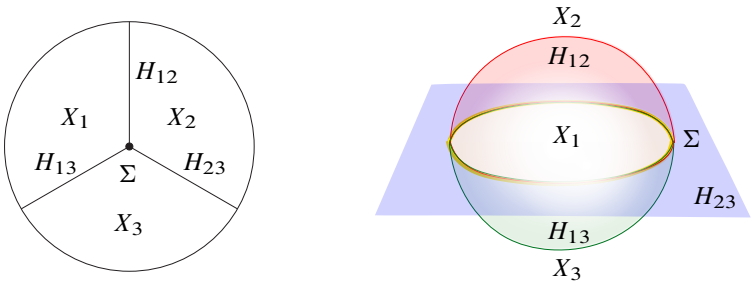

Figure 10. (a) Schematic representation of the trisection of a 4-manifold M. X_1, X_2, and X_3 are four-dimensional submanifolds whose boundaries are $H_{12} \cup H_{13}$, $H_{12} \cup H_{23}$, and $H_{13} \cup H_{23}$, respectively. H_{12}, H_{13}, and H_{23} are three-dimensional handlebodies and Σ is a Heegaard surfaces for the pairs $\{H_{12}, H_{13}\}$, $\{H_{12}, H_{23}\}$, and $\{H_{13}, H_{23}\}$. Σ is called the central surface of a trisection. (b) Lower three-dimensional representation of the trisected manifold. H_{12} is represented in half of S^2 colored in red, H_{13} in green, and H_{23} in blue surface. Inside of S^2, namely D^3 bounded by H_{12} and H_{13} represents X_1, whereas the outside space above (below) H_{12} (H_{13}) and H_{23} represents X_2 (X_3). The yellow circle represents Σ. This representation of a trisection is very crude and strictly speaking wrong (e.g., keep in mind that M ought to be closed); obviously, all the submanifolds and the given manifold itself are in principle general, however in this representation, they are depicted in a very special way.

of curves: α-curves, β-curves and γ-curves (collectively, attaching curves). These curves are constructed, as before, by means of compression discs and represent the belt spheres of the 1-handle of each of the three-dimensional handlebodies H_{ij}. A trisection diagram therefore combines the three Heegaard diagrams for ∂X_i into a single diagram. Thus one can say that the construction of trisection, together with the extending theorem, allows us to study four-dimensional topology, within a two-dimensional framework. Again, infinitely many possible trisection diagrams are viable for a given manifold and they are connected by a finite sequence of moves generalizing Heegaard moves. Therefore, we have the following:

Definition 4.3. Given a 4-manifold M, the minimal genus over all the possible central surfaces trisecting M is a topological invariant. We call this number *trisection genus*.

We remark that the connected sum of two 4-manifolds $M = \{H_{12}, H_{23}, H_{13}, \Sigma_M\}$ (defining implicitly the handlebodies X_1, X_2 and X_3) and $N = \{K_{12}, K_{23}, K_{13}, \Sigma_N\}$ (defining Y_1, Y_2 and Y_3) can be constructed in analogy to the three-dimensional case by removing 4-balls which intersect all the elements of each trisection in balls of the appropriate dimension. The resulting manifold will support a trisection of the form $M \sharp N = \{H_{12} \natural K_{12}, H_{23} \natural K_{23}, H_{13} \natural K_{13}, \Sigma_M \sharp \Sigma_N\}$ implicitly defining the handlebodies $X_1 \natural Y_1$, $X_2 \natural Y_2$ and $X_3 \natural Y_3$.

4.1. Stabilization

Both in the context of Heegaard splittings and of trisections there is a move that increases the genus of the central surface by one. It is instructive to illustrate how this can be achieved and to point out small differences between the four-dimensional and three-dimensional cases.

We consider a three-dimensional manifold $M^{(3)}$ with a Heegaard diagram of genus g, Σ_M, and the genus-1 Heegaard diagram of S^3, which we call T_S (see Figure 4). Since S^3 has trivial topology we have the following identity:

$$M^{(3)} \sharp S^3 = M^{(3)}.$$

As explained in Section 3.2, this operation can be represented by the diagram $\Sigma_M \sharp T_S$ which has genus $g' = g + 1$. We can understand this operation in terms of carving a handle out of one of the two handlebodies in $M^{(3)}$ and adding it to the other one. For a given d-manifold N with boundary, the operation of drilling out a tubular neighborhood of a properly embedded ball $D^{d-k-1} \subset N$ is equivalent to adding a k-handle whose attaching sphere bounds a ball D^k in ∂N. The properly embedded $(d-k-1)$-ball is bounded by the belt sphere of a $(k+1)$-handle which we may add in order to cancel the k-handle and to recover N. This describes how to increment the genus of the central surface of a Heegaard diagram if we consider the case[12] $d = 3$ and $k = 1$; note that a 2-handle for one handlebody plays the role of a 1-handle for the other handlebody. In this way, it is clear how we are actually not changing anything in the overall manifold but rather rearranging its handle decomposition.

In four dimensions there exist a similar operation which is called *stabilization*. The genus-1 trisection diagrams of S^4 are shown in Figure 11 (b) and each represents a trisection where two handlebodies X_i and X_j are 4-balls while the third X_k has genus-1. Note that the boundary ∂X_k has the topology of $S^1 \times S^2$ as can be seen from each diagram by removing the curve circulating around the toroidal direction.

If we consider a 4-manifold $M^{(4)}$ we can clearly increment the genus of its central surface by considering the connected sum of its trisection diagram with one of the three in Figure 11 (b). Although this is not within the investigation scope of the present work, we should mention that the stabilization operation allows us to always

[12]Note that for $k = 1$ we identify two discs on the boundary of a handlebody and represent their identification through the spine of the resulting 1-handle. From this point of view, we can treat the operation of increasing the genus of a handlebody and the connected sum of two handlebodies (see Figure 6) on the same footing, with the only difference being whether the considered discs lie on the boundary of the same handlebody or not. Note that in both cases it is sufficient to specify the spine of the new handle in order to recover the full topological information.

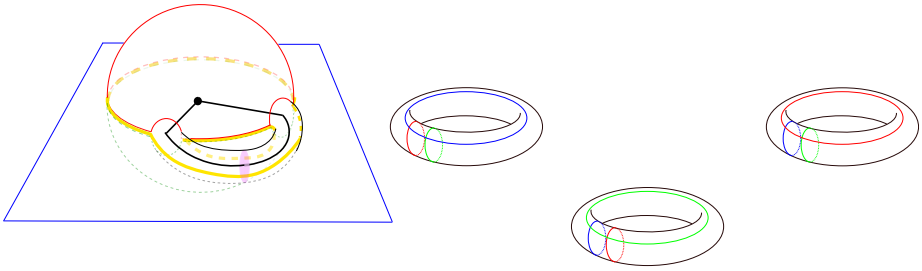

(a) (b)

Figure 11. Lower-dimensional (in three dimensions) representation of stabilization in four dimensions. Figure 11 (a) represents the process of adding a four-dimensional 1-handle to one of the handlebodies preserving the trisection structure. The figure follows the conventions of Figure 10 (b). We also show the resulting spine of the four-dimensional handlebody as well as the compression disc for the new handle. Figure 11 (b) shows the three genus-1 trisection diagrams for S^4. Stabilization can be represented at the level of trisection diagrams as the connected sum with one of these three diagrams.

obtain a trisection where all the four-dimensional handlebodies have the same genus. This type of trisection is referred to as *balanced*. In fact, it is worth noticing that the stabilization operation, although affecting the topology of all the three-dimensional handlebodies H_{ij}, only affects one of the four-dimensional ones, while leaving the other two unmodified.

Stabilization too can be understood as a specific carving operation. As before, we identify a D^1 that constitutes the spine of the carved 1-handle. Since we are going to increase the genus of, say, X_1, the 1-ball will need to be properly embedded in the complement $M^{(4)} \setminus X_1$ (we will carve the handle out of the complement and add it to X_1). The central surface simultaneously represents the boundary of all the three-dimensional handlebodies which, therefore, need to have their genus increased as well. Since we are only specifying one 1-handle, and with simple symmetry considerations, it is easy to guess that the spine should be a disc D^1 embedded in H_{23}, with endpoints on the central surface. Figure 11 shows a schematic representation of this procedure following the same conventions of Figure 10 (b). Under such a move, the topology of X_2 and X_3 remains unaffected. To understand this, it is sufficient to notice that X_2 in Figure 10 (b) (resp. X_3) intersects only half of the 1-handle and the intersection is a 4-disc intersecting ∂X_2 (resp. ∂X_3) in D^3 (see Figure 11). In other words, carving the 1-handle leads to two manifolds X_2' and X_3' satisfying:

$$X_2' \natural D^4 = X_2, \quad X_3' \natural D^4 = X_3.$$

Note that the portion of the boundary of the four-dimensional 1-handle that does not constitute the attaching sphere has the topology of $D^1 \times S^2$. Upon the following decomposition

$$D^1 \times S^2 = (D^1 \times D^2) \bigcup_{D^1 \times S^1} (D^1 \times D^2),$$

we can understand it as a pair of three-dimensional 1-handles with common boundaries and "parallel" spines. Therefore, a regular neighborhood of a one-dimensional disc properly embedded in one of the three-dimensional handlebodies intersects all the elements of a trisection without spoiling the construction, but rather defining an alternative trisection for the same manifold.

4.2. Subdividing 4-simplices

We would like to understand trisections from *colored triangulations*, i.e., triangulations dual to colored graphs which can be generated by colored tensor models. It amounts to formulating trisections relying on combinatorics. We will do so, by generalising the three-dimensional Heegaard splittings formulated in the colored tensor models [103]. From now on, we therefore restrict to the PL category.

Following [3], let us consider a 4-simplex $\Delta^{(4)}$ and define a partition of its vertices in three sets P_0, P_1 and P_2 such that one vertex belongs to one of the sets and the rest is divided in two pairs. For example, labeling each vertex with the color of its opposite 3-face we might have that the vertex $v^{\hat{0}}$ is assigned to P_0, the vertices $v^{\hat{1}}$ and $v^{\hat{2}}$ are assigned to P_1 and the vertices $v^{\hat{3}}$ and $v^{\hat{4}}$ are assigned to P_2. Given such a partition, any pair of sets (P_i, P_j) is identified with a n-dimensional subsimplex on the boundary of $\Delta^{(4)}$ while the third set P_k is identified with the opposite $(3-n)$-dimensional subsimplex, where $i, j, k \in \{0, 1, 2\}$ and $i \neq j \neq k$. For example, $(P_1 = \{v^{\hat{1}}, v^{\hat{2}}\}, P_2 = \{v^{\hat{3}}, v^{\hat{4}}\})$ and $P_0 = \{v^{\hat{0}}\}$ give a 3-simplex spanned by $v^{\hat{1}}$, $v^{\hat{2}}$, $v^{\hat{3}}$, $v^{\hat{4}}$ and a 0-simplex $v^{\hat{0}}$, whereas $(P_0 = \{v^{\hat{0}}\}, P_1 = \{v^{\hat{1}}, v^{\hat{2}}\})$ and $P_2 = \{v^{\hat{3}}, v^{\hat{4}}\}$ give a 2-simplex spanned by $v^{\hat{0}}$, $v^{\hat{1}}$, $v^{\hat{2}}$ and a 1-simplex with endpoints $v^{\hat{3}}$ and $v^{\hat{4}}$.

Then, we can define a map f from $\Delta^{(4)}$ to $\Delta^{(2)}$ such that each set P_i is sent into each of the three vertices in $\Delta^{(2)}$ and extend it linearly to the interiors of $\Delta^{(4)}$ and $\Delta^{(2)}$. We proceed by considering the subcomplex spanned by the 0-skeleton of the first barycentric subdivision of $\Delta^{(2)}$ minus the 0-skeleton of $\Delta^{(2)}$. The resulting cubical decomposition of $\Delta^{(2)}$ is shown in Figure 12. $\Delta^{(2)}$ is decomposed in three 2-cubes c_i with $i \in 1, 2, 3$, pairwise intersections of which result in 1-cubes c_{ij}, all sharing a central 0-cube, c_{123}. The preimage of this construction under f gives us the splitting of $\Delta^{(4)}$ we are looking for. Notice that the boundary faces of $\Delta^{(2)}$ (each spanned by two vertices) are subdivided into two 1-cubes. The preimage of f therefore induces splittings of the subsimplices on the boundary of $\Delta^{(4)}$ identified with the pairs (P_i, P_j). Focusing on $\Delta^{(3)} \ni \{v^{\hat{1}}, v^{\hat{2}}, v^{\hat{3}}, v^{\hat{4}}\}$, which is sitting opposite to $v^{\hat{0}}$, and

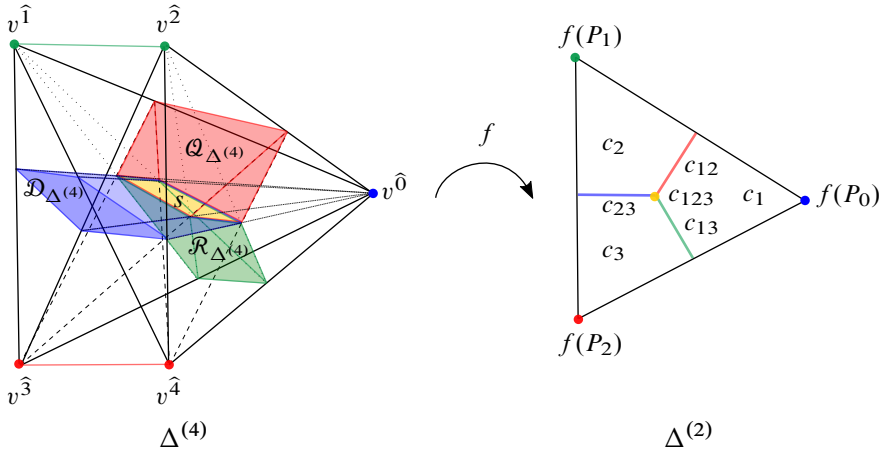

Figure 12. Illustration of the linear map from $\Delta^{(4)}$ to $\Delta^{(2)}$. The sets P_i partitioning the vertices of the 4-simplex $\Delta^{(4)}$, as well as their images in 2-simplex $\Delta^{(2)}$, are shown. Removing the 0-skeleton of $\Delta^{(2)}$ from the 0-skeleton of its first barycentric subdivision provides with the cubical decomposition. The preimage of $\Delta^{(2)}$ under f splits the 4-simplex in three four-dimensional pieces, whose boundaries are three-dimensional blocks $\mathcal{D}_{\Delta^{(4)}}$, $\mathcal{Q}_{\Delta^{(4)}}$, and $\mathcal{R}_{\Delta^{(4)}}$. The latter three three-dimensional blocks meet at one two-dimensional square s. $\mathcal{D}_{\Delta^{(4)}}$ is in blue, $\mathcal{Q}_{\Delta^{(4)}}$ in red, $\mathcal{R}_{\Delta^{(4)}}$ in green, and the common surface s in yellow. $f(\mathcal{D}_{\Delta^{(4)}}) = c_{23}$, $f(\mathcal{Q}_{\Delta^{(4)}}) = c_{12}$, $f(\mathcal{R}_{\Delta^{(4)}}) = c_{13}$, and $f(s) = c_{123}$.

considering the partition $P_1 = \{v^{\hat{1}}, v^{\hat{2}}\}$, $P_2 = \{v^{\hat{3}}, v^{\hat{4}}\}$ and $P_0 = \{v^{\hat{0}}\}$, $\Delta^{(3)}$ is mapped via f to a 1-simplex of $\Delta^{(2)}$ in precisely the same manner as in Figure 7. The coning of the splitting surface of $\Delta^{(3)}$ with respect to $v^{\hat{0}}$, generates a square prism which we call $\mathcal{D}_{\Delta^{(4)}}$, whose image under f is 1-cube c_{23}. Similarly, in the two 2-subsimplices of $\Delta^{(4)}$ defined by $\{P_0, P_1\}$ and $\{P_0, P_2\}$, we identify a one-dimensional cross section, which then will be coned toward P_2 and P_1, respectively. These conings generate triangular prisms $\mathcal{Q}_{\Delta^{(4)}}$ and $\mathcal{R}_{\Delta^{(4)}}$, whose images are c_{12} and c_{13} in $\Delta^{(2)}$. The intersection $\mathcal{Q}_{\Delta^{(4)}} \cap \mathcal{R}_{\Delta^{(4)}} \cap D_{\Delta^{(4)}}$ is a two-dimensional cube.[13] Figure 12 shows such coning operations.

4.3. Splitting 4-bubbles

At this point, one would like to induce the above subdivision in every simplex σ of a triangulation $\mathcal{T}$ of a given manifold M and prove the emerging structure of a trisection, namely see that each of the sets $\mathcal{D} = \bigcup_\sigma \mathcal{D}_\sigma$, $\mathcal{Q} = \bigcup_\sigma \mathcal{Q}_\sigma$, $\mathcal{R} = \bigcup_\sigma \mathcal{R}_\sigma$

[13]The bidimensionality of the central square is ensured by the fact that all the pairwise intersections of the three-dimensional blocks are transverse.

is connected and homeomorphic to a handlebody. In order to achieve this[14] we will have to perform a few manipulations. For later reference, we call the attaching curves determined by manipulations of $\mathcal{Q}$ (resp. $\mathcal{R}$, $\mathcal{D}$) as α (resp. β, γ).

Let us consider a colored triangulation $\mathcal{T}$ of a 4-manifold M, and a colored graph $\mathcal{G}$ dual to $\mathcal{T}$, i.e., $K(\mathcal{G}) = \mathcal{T}$ and $|K(\mathcal{G})| = M$. If we take seriously a partition of the vertices induced by colors, we notice soon that the main immediate obstacle is achieving the connectedness of $\mathcal{Q}$ and $\mathcal{R}$. Evidently, the union $\mathcal{Q} \cup \mathcal{R}$ consists of disconnected three-dimensional polytopes surrounding the vertices of $\mathcal{T}$ which belong to the isolated partition set whose element is only one vertex per 4-simplex.

Let us elaborate on the structure of $\mathcal{Q}$ and $\mathcal{R}$. In the triangulation $\mathcal{T}$, a 4-bubble $\mathcal{B}_a^{\hat{i}}$ identifies a three-dimensional subcomplex which surrounds a vertex $v_a^{\hat{i}}$. In particular, $v_a^{\hat{i}}$ sits opposite to a 3-face of color i in every 4-simplex containing it and the triangulation dual to $\mathcal{B}_a^{\hat{i}}$, $K(\mathcal{B}_a^{\hat{i}})$, is PL-homeomorphic to the union of such 3-faces. Moreover, we point out that such a triangulation, $K(\mathcal{B}_a^{\hat{i}})$, is also homeomorphic to the link of $v_a^{\hat{i}}$ which, for the case of M being a manifold, turns out to be a topological 3-sphere.[15] See Figure 13 for a lower-dimensional representation of $K(\mathcal{B}^{\hat{0}})$. Given the combination of colors defining the 4-bubble, a possibly more accurate way to address the corresponding triangulation is not as the union of the 3-faces situating opposite to $v_a^{\hat{i}}$, but rather as the union of a set of three-dimensional cross sections parallel to such 3-faces which cut 4-simplices midway between $v_a^{\hat{i}}$ and its opposite 3-faces, namely, $\mathcal{Q}_{\sigma_a} \cup \mathcal{R}_{\sigma_a}$ in Figure 14.

Consequently, given the set $\Delta_a = \{\sigma \text{ 4-simplex s.t. } v_a^{\hat{i}} \in \sigma\}$, the 4-bubble identifies the union

$$K(\mathcal{B}_a^{\hat{i}}) = \bigcup_{\sigma \in \Delta_a} \mathcal{Q}_\sigma \cup \mathcal{R}_\sigma.$$

For later reference, we call the four-dimensional neighborhood[16] of $v_a^{\hat{0}}$ bounded by $K(\mathcal{B}_a^{\hat{0}})$, X_1^a and we define the following unions:

$$\mathcal{Q}_a = \bigcup_{\sigma \in \Delta_a} \mathcal{Q}_\sigma, \quad \mathcal{R}_a = \bigcup_{\sigma \in \Delta_a} \mathcal{R}_\sigma.$$

[14] Indeed, we have to define a new structure related to $\mathcal{D}$, which improves its topological properties in order to obtain a handlebody.

[15] Nevertheless, colored tensor models and colored graphs generate in general pseudomanifolds and, therefore, the topology of $K(\mathcal{B}_a^{\hat{i}})$ might turn out to be very different. We comment on this case in Section 4.7.

[16] Note that we choose to call this X_1^a as it will be part of one of the trisection four-dimensional handlebodies defined earlier in Definition 4.1.

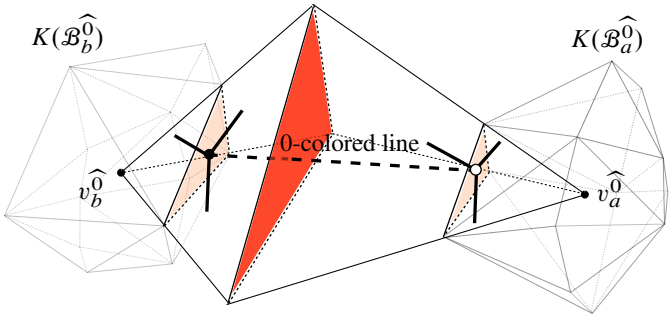

Figure 13. Representation of two components of $K(\mathcal{B}^{\hat{0}})$ in a three-dimensional complex. In three dimensions, $K(\mathcal{B}^{\hat{0}})$ is a two-dimensional complex whose edges are shown in grey. In the picture we present two components: $K(\mathcal{B}_a^{\hat{0}})$ and $K(\mathcal{B}_b^{\hat{0}})$, surrounding $v_a^{\hat{0}}$ and $v_b^{\hat{0}}$, respectively. The same 0-colored face (shown in red and shared by two 3-simplices) gives rise to two different building blocks (shown in orange) in $K(\mathcal{B}^{\hat{0}})$.

We pick 0 as a special color and define a specific partition,[17] i.e., $P_0 = \{v^{\hat{0}}\}$, $P_1 = \{v^{\hat{1}}\} \cup \{v^{\hat{2}}\}$ and $P_2 = \{v^{\hat{3}}\} \cup \{v^{\hat{4}}\}$. Then we consider the 4-bubbles $\mathcal{B}_a^{\hat{0}}$ and, in each such 4-bubble, the jacket $\mathcal{J}_{P_1,P_2} = \mathcal{J}_{\{1,2\},\{3,4\}}$. Combining the constructions described in Sections 3.3 and 4.2, we readily obtain the sets $\mathcal{Q}$ and $\mathcal{R}$. Nevertheless, each of these sets, is disconnected and constituted by as many connected components as many vertices $v^{\hat{0}}$ are in the triangulation $\mathcal{T}$. Recalling how jackets identify Heegaard surfaces for the realizations of 4-colored graphs, it is easy to see that $\mathcal{Q}_a$ and $\mathcal{R}_a$ are the two handlebodies in a Heegaard splitting of a given $\mathcal{B}_a^{\hat{0}}$. Looking at the Heegaard splittings $\mathcal{B}_a^{\hat{0}} = (H_{1,a}, H_{2,a}, K(\mathcal{J}(\mathcal{B}_a^{\hat{0}})))$, we have that:

$$\mathcal{Q}_a = H_{1,a}, \quad \mathcal{R}_a = H_{2,a}, \quad \mathcal{Q} = \bigsqcup_a H_{1,a}, \quad \mathcal{R} = \bigsqcup_a H_{2,a},$$

with $\sqcup$ representing the disjoint union of sets.

It is now clear that there is a limitation of partitioning the vertices in the triangulation according to colors if we try to identify a trisection naively. Moreover, the information on $\mathcal{D}$, although formally present, appears to be implicit and hidden in the construction. In previous works [3], as we briefly mentioned, these problems have been tackled in two different ways. In [3], the authors perform Pachner moves on the triangulation. The specific type of Pachner move employed ($2 \to 4$ Pachner move)

[17] Here we picked the color 0 to identify the vertex that in every 4-simplex is "isolated" by the partition, nevertheless, we stress that at this level any permutation of the colors would be an equivalent choice.

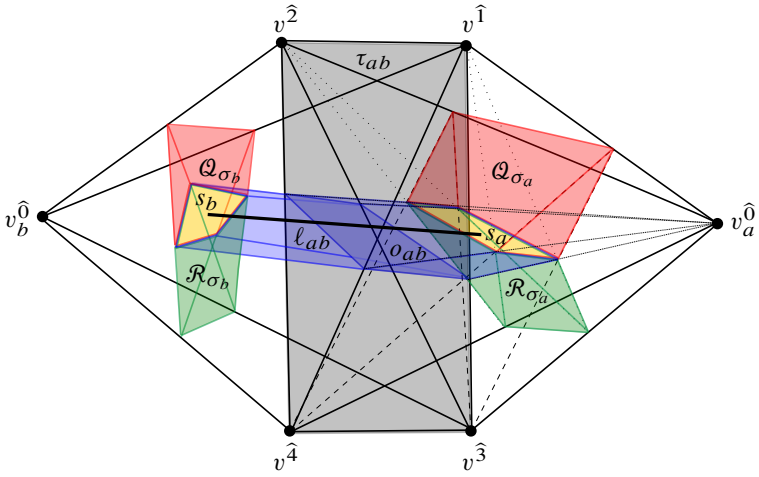

Figure 14. Representation of π_{ab}. The picture shows the combinatorial structure of the polytope resulting from two 4-simplices, σ_a and σ_b, sharing one boundary 0-colored face τ_{ab} spanned by $\{v^{\hat{1}}, v^{\hat{2}}, v^{\hat{3}}, v^{\hat{4}}\}$. Each $\sigma_i, i = a, b$, can be considered as the coning of τ_{ab} with respect to $v_i^{\hat{0}}$. The tetrahedron τ_{ab} is split by the square o_{ab}, depicted in dark violet. Moreover, each 4-simplex is split by the three-dimensional $\mathcal{Q}_{\sigma_i}$, $\mathcal{R}_{\sigma_i}$, $\mathcal{D}_{\sigma_i}$, here in red, green and violet, respectively. We represent in yellow the two squares s_a and s_b that contribute to the central surfaces of each 4-bubble $\mathcal{B}_a^{\hat{0}}$ and $\mathcal{B}_b^{\hat{0}}$. The thick black line in the center of the figure is the embedded 0-colored line l_{ab} connecting s_a and s_b.

increases the number of 4-simplices in $\mathcal{T}$ without affecting the topology (replaces a 4-ball by another 4-ball having the same triangulation on the boundary). This allows to connect the spines of the four-dimensional handlebodies at will, as well as to clearly infer the structure of compression discs for all the three-dimensional handlebodies. Nevertheless, Pachner moves are not compatible with the colors in the present case, since the complete graph with six vertices cannot be consistently 5-colored. On the other hand, in [29] the authors considered a special class of colored graphs encoding crystallizations. By definition, all $K(B^{\hat{i}})$ are connected in crystallization theory. Such requirement imposes a limited amount of nodes in the graph encoding a manifold M, which results in a very powerful tool to study the topology of PL-manifolds.[18] However, crystallization graphs only reflect a small amount of cases of interest to the tensor model community. In the following section we present an alternative approach which allows to generalize the construction of trisections to a wider class of graphs.

[18] As we will explain later, the authors of [29] actually consider a wider class of graphs. Nevertheless, they still base their construction on connectedness of some chosen $\hat{i}$-bubble.

4.4. Connecting 4-bubbles

In order to overcome the issues coming from having disconnected realizations of 4-bubbles, we follow a similar construction of Heegaard splittings discussed in Section 3.4. Let us start by embedding the colored graph dual to $\mathcal{T}$ in $\mathcal{T}$ itself via the prescription described in Section 2.1. We consider four-dimensional regular neighborhoods of the 0-colored lines embedded in $\mathcal{T}$. Topologically, each such four-dimensional neighborhood n is $\mathrm{D}^3 \times \mathrm{D}^1$, and its boundary is $(\mathrm{S}^2 \times \mathrm{D}^1) \cup (\mathrm{D}^3 \times \mathrm{S}^0)$. This boundary intersects $\mathcal{D}$ (three-dimensional) transversally and, therefore, the longitudinal component $\mathrm{S}^2 \times \mathrm{D}^1$ is split by $\mathcal{D}$ into two parts: $\partial_+ n$ and $\partial_- n$, each of topology $\mathrm{D}^2 \times \mathrm{D}^1$. As a convention we fix $\partial_+ n$ to be between $\mathcal{D}$ and $\{v^{\widehat{1}}, v^{\widehat{2}}\}$ and $\partial_- n$ between $\mathcal{D}$ and $\{v^{\widehat{3}}, v^{\widehat{4}}\}$.

Construction 4.4. *Given a colored triangulation $\mathcal{T}$ of a manifold M, dual to a colored graph $\mathcal{G}$, and a choice of a jacket for its $\widehat{0}$-bubbles, $\mathcal{J}(\mathcal{B}^{\widehat{0}}_a)$, there exist three 3-submanifolds of $\mathcal{T}$: $\mathcal{Q}'$, $\mathcal{R}'$ and $\mathcal{D}'$, such that they share the same boundary*

$$\Sigma = \partial\mathcal{Q}' = \partial\mathcal{R}' = \partial\mathcal{D}',$$

and which are constructed carving regular neighborhoods of the embedded 0-colored lines of $\mathcal{G}$ as

$$\begin{aligned}
\mathcal{Q}' &= \Big[\mathcal{Q} \setminus \Big(\bigcup_l n\Big)\Big] \cup \Big[\bigcup_l \partial_+ n\Big],\\
\mathcal{R}' &= \Big[\mathcal{R} \setminus \Big(\bigcup_l n\Big)\Big] \cup \Big[\bigcup_l \partial_- n\Big],\\
\mathcal{D}' &= \mathcal{D} \setminus \Big[\bigcup_l \dot{n}\Big],
\end{aligned}$$

where l runs over the set of 0-colored lines and $\dot{n}$ indicates the interior of n.

In order to understand Construction 4.4, let us consider two vertices $v^{\widehat{0}}_a$ and $v^{\widehat{0}}_b$ sitting opposite to the same 0-colored 3-face, τ_{ab} and call n_{ab}, the regular neighborhood of the 0-colored line ℓ_{ab} dual to τ_{ab}. We call the 4-simplex spanned by $v^{\widehat{0}}_a \cup \tau_{ab}$, σ_a, and similarly for b.

One can view the 3-ball D^3 in this four-dimensional regular neighborhood of a 0-colored line, n_{ab}, as a retraction of the tetrahedron $\mathcal{Q}_{\sigma_a} \cup \mathcal{R}_{\sigma_a} = K(\mathcal{B}^{\widehat{0}}_a) \cap \sigma_a$ (or for b) inside each 4-simplex, σ_a (or σ_b), where $\mathcal{Q}_{\sigma_a}$ is $\mathcal{Q} \cap \sigma_a$, etc. Using n_{ab}, we perform a connected sum of the 3-submanifolds defined by 4-bubbles $K(\mathcal{B}^{\widehat{0}})$'s and, at the same time, perform a boundary-connected sum of the four-dimensional neighborhoods of vertices in the triangulation.

The union $\sigma_a \cup \sigma_b$ via their shared face τ_{ab} defines a polytope[19] π_{ab}, spanned by $v_a^{\hat{0}} \cup \tau_{ab} \cup v_b^{\hat{0}}$. In each π_{ab}, there are two central squares s_a and s_b which are the intersections of π_{ab} with the realization of jackets of $\hat{0}$-bubbles $K(\mathcal{J}(\mathcal{B}_a^{\hat{0}}))$ and $K(\mathcal{J}(\mathcal{B}_b^{\hat{0}}))$, respectively. We note that a neighborhood of the barycenter of s_a (resp. s_b) intersects $K(\mathcal{B}_a^{\hat{0}})$ (resp. $K(\mathcal{B}_b^{\hat{0}})$) in a 3-ball satisfying the requirements presented in Section 3.2. Therefore, by removing such neighborhoods and identifying their boundaries, we can easily construct the connected sum $K(\mathcal{B}_a^{\hat{0}}) \sharp K(\mathcal{B}_b^{\hat{0}})$ preserving the Heegaard splitting defined by the chosen jackets, i.e., connecting the components of $\mathcal{Q}$ (resp. $\mathcal{R}$) surrounding $v_a^{\hat{0}}$ and $v_b^{\hat{0}}$. For later convenience, we require the neighborhood of the barycenter of s_a (resp. s_b) to be small enough not to intersect ∂s_a (resp. ∂s_b). Note that, by construction, this also yields $X_1^a \natural X_1^b$. As we discussed in Section 3.2, we can represent the boundary-connected sum of handlebodies through a line connecting the boundaries. This is precisely the role of ℓ_{ab}; $X_1^{ab} = X_1^a \cup n_{ab} \cup X_1^b$ is homeomorphic to $X_1^a \natural X_1^b$. The intersections $q_a = s_a \cap n_{ab}$ and $q_b = s_b \cap n_{ab}$ identify smaller squares splitting each D^3 in $(\mathrm{D}^3 \times \mathrm{S}^0) \subset \partial n_{ab}$. The interiors of q_a and q_b now belong to the interior of X_1^{ab} while their boundaries define a surface

$$\Sigma_{ab} = \partial q_a \times \ell_{ab} = \partial q_b \times \ell_{ab}.$$

It is now straightforward to see that we just constructed the connected sum of the surfaces dual to $\mathcal{J}(\mathcal{B}_a^{\hat{0}})$ and $\mathcal{J}(\mathcal{B}_b^{\hat{0}})$ by simply considering the following union:

$$[K(\mathcal{J}(\mathcal{B}_a^{\hat{0}})) \setminus q_a] \cup \Sigma_{ab} \cup [K(\mathcal{J}(\mathcal{B}_b^{\hat{0}})) \setminus q_b].$$

With a similar construction and following the arguments of Section 3.2, it is not hard to see that we also constructed the boundary-connected sums $\mathcal{Q}_{\sigma_a} \natural \mathcal{Q}_{\sigma_b}$ and $\mathcal{R}_{\sigma_a} \natural \mathcal{R}_{\sigma_b}$. Notice that the boundary-connected sum of the three-dimensional handlebodies is made preserving the combinatorics defined by the chosen jacket, and this clarifies any ambiguity due to a choice of orientation.

Since ℓ_{ab} is transversal to τ_{ab}, it is easy to see that it lies inside $\mathcal{D}_{\sigma_a} \cup \mathcal{D}_{\sigma_b}$. The intersections $(n_{ab} \cap \mathcal{D}_{\sigma_a}) \cup (n_{ab} \cap \mathcal{D}_{\sigma_b})$ identify what shall be carved out of $\mathcal{D}_{\sigma_a}$ and $\mathcal{D}_{\sigma_b}$. Here, we require $(n_{ab} \cap \partial\mathcal{D}_{\sigma_a}) = \emptyset$ (and similarly for $\partial\mathcal{D}_{\sigma_b}$) in order to avoid singularities. The operation is, thus, very similar to a stabilization up to the fact that we are identifying balls on the boundaries of two disconnected handlebodies. The boundary of the (three-dimensional) carved region in $\mathcal{D}_{\sigma_a} \cup \mathcal{D}_{\sigma_b}$ is, again, Σ_{ab}. Hence, Σ_{ab} is identified as the central surface obtained through such a carving operation.

[19] They are called a double pentachora in [3].

In general, there are more than one 0-colored 3-faces sitting opposite to the same pair $v_a^{\widehat{0}}$ and $v_b^{\widehat{0}}$; we denote this number E_{ab}. It means that there are E_{ab}-many embedded 0-colored lines connecting the two realizations of the bubbles $K(\mathcal{B}_a^{\widehat{0}})$ and $K(\mathcal{B}_b^{\widehat{0}})$. Repeating the above procedure for all E_{ab} lines not only defines the boundary-connected sums $\mathcal{Q}_a \natural \mathcal{Q}_b$ and $\mathcal{R}_a \natural \mathcal{R}_b$, but also adds to each of them $E_{ab} - 1$ extra 1-handles via stabilization.

We are left to clarify how $\mathcal{D} = \bigcup_\sigma \mathcal{D}_\sigma$ behaves under the iterated carving operation. Let us first notice that each $\mathcal{D}_\sigma$ is bounded by six rectangular faces. One, as we defined earlier, is s and is determined by the intersection of σ with the realization of a jacket of a $\widehat{0}$-bubble. The surface s is the only face of $\mathcal{D}_\sigma$ whose interior lies in the interior of σ. The interior of the other five faces lies inside the interior of one of the five boundary faces of σ. Hence, each boundary face of $\mathcal{D}_\sigma$ naturally carries a single color from the colored graph $\mathcal{G}$. The face carrying the color 0 is the one sitting opposite to s and we call it o. For every $\mathcal{D}_\sigma$ in M there is one and only one $\mathcal{D}_{\sigma'}$ sharing o with $\mathcal{D}_\sigma$. The union $\mathcal{D}_\sigma \cup \mathcal{D}_{\sigma'}$ can be thought of as the effective building blocks of $\mathcal{D}$ and they are in one to one correspondence with the 0-colored lines of $\mathcal{G}$. These building blocks are also bounded by ten faces; in π_{ab}, we have: s_a, s_b, four lateral faces carrying colors $i \neq 0$ coming from $\mathcal{D}_{\sigma_a}$ and four lateral faces carrying colors $i \neq 0$ coming from $\mathcal{D}_{\sigma_b}$. Note that faces of the same color coming from $\mathcal{D}_{\sigma_a}$ and $\mathcal{D}_{\sigma_b}$ are glued to each other via a boundary edge. When we compose such blocks to build $\mathcal{D}$, each block glues to another sharing a lateral face according to the colors.

It is important to realize that the embedding of 0-colored lines connects opposite faces of such building blocks, namely s_a and s_b, therefore a tubular neighborhood of a 0-colored line always intersects s_a and s_b. After carving such neighborhoods out of $\mathcal{D}$, each building block is turned into a solid torus (pictorially, we can think of tunneling through them along a 0-colored line, see Figure 15 (a)). In π_{ab}, we refer to such new effective building blocks as

$$\mathcal{D}_{ab}^{(\ell)} = (\mathcal{D}_{\sigma_a} \cup \mathcal{D}_{\sigma_b}) \setminus n_{ab},$$

and the resulting entire structure corresponds to

$$\mathcal{D}' = \mathcal{D} \setminus \left(\bigcup_{\ell_{ab}} n_{ab} \right) = \bigcup_{\ell_{ab}} \mathcal{D}_{ab}^{(\ell)} = \natural \mathcal{D}_{ab}^{(\ell)}.$$

Before moving on, an important remark is in order. So far we discussed the case of $v_a^{\widehat{0}}$ is different from $v_b^{\widehat{0}}$. Nevertheless, it may easily happen that τ_{ab} opposes to the same $\widehat{0}$-colored vertex (in fact, it is sufficient that the two 4-simplices in π_{ab} share one more face, beside τ_{ab}, for this to be true). In this case, as explained in Section 4.1, most of the features we just discussed would still hold. Simply, instead

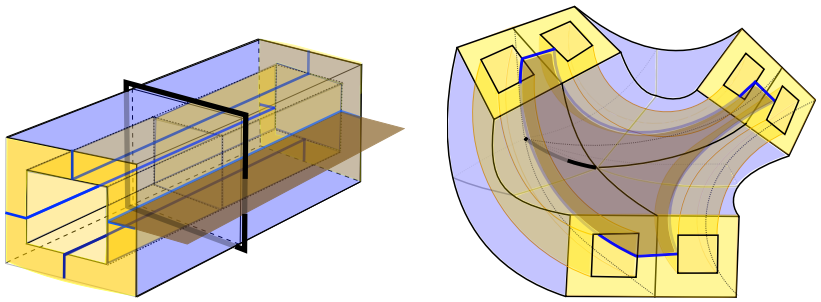

(a) (b)

Figure 15. Structure of $\mathcal{D}'$. Figure 15 (a) shows an effective building block of $\mathcal{D}'$, namely $\mathcal{D}^{(\ell)}_{ab}$. There are eight blue 2-faces which are to be glued to other effective building blocks of $\mathcal{D}'$. The yellow surface is going to be part of the central surface of the trisection and, therefore, will constitute the boundary of $\mathcal{D}'$, i.e., to be glued onto $\mathcal{Q}$ and $\mathcal{R}$. Four pieces of the γ-curves describing $\mathcal{D}'$ are pictured in blue lines. The brown rectangle with one of the γ-curves as boundary represents part of a compression disc. The spine of the effective block of $\mathcal{D}'$ is shown in thick solid black loop piercing through the compression disc. Figure 15 (b) shows three effective building blocks of $\mathcal{D}'$ glued along their i-colored faces (let us pick $i = 1$). Here we show a γ-curve in blue, circulating along all of the three effective building blocks and defining the boundary of a compression disc (shown in brown). In this example, the γ-curve is defined by the color set $\{0, 1\}$. All the other γ-curves, which we do not show, only travel through one block and then move away on other patches of the central surface which are not shown in the picture. As before, patches of the central surface are shown in yellow an lateral faces in blue.

of performing a connected sum between two $\hat{0}$-bubbles, we would be adding a 1-handle to a single $\hat{0}$-bubble via stabilization (as in Figure 11) and increase by one the genus of the central surface defined by $K(\mathcal{J}(\mathcal{B}^{\hat{0}}_a))$. In particular, this situation would correspond to a single building block $\mathcal{D}^{(\ell)}_{ab}$ in which two lateral faces of the same color i are identified. One can understand such operation as the retraction to a point of a disc on the boundary of $\mathcal{D}^{(\ell)}_{ab}$, bounded by a trivial element in the first homotopy group of the 2-torus.[20] Topologically, such $\mathcal{D}^{(\ell)}_{ab}$ would therefore remain a solid torus.

We are now ready to state the main result of this work.

Theorem 4.5. *$\mathcal{Q}'$, $\mathcal{R}'$ and $\mathcal{D}'$ are handlebodies.*

Proof. The submanifolds $\mathcal{Q}'$ and $\mathcal{R}'$, as explained in Construction 4.4, are stabilizations of the boundary-connected sum of the handlebodies $\{\mathcal{Q}_a\}$ and $\{\mathcal{R}_a\}$, respectively, and, as such, are handlebodies themselves. Their spines are defined as described

[20] Remember that two faces of the same color in $\mathcal{D}^{(\ell)}_{ab}$ already share a side.

in Sections 3.2, 3.3 and 4.1, i.e., via the bicolored paths defining the jacket, joined by the embedded 0-colored lines of $\mathcal{G}$.

Note that $\mathcal{D}'$ coincides with the boundary-connected sum of the building blocks $\mathcal{D}^{(\ell)}_{ab}$ performed via their lateral faces. Since the $\mathcal{D}^{(\ell)}_{ab}$ are solid tori, $\mathcal{D}'$ is a handlebody by construction. The prescription to perform such boundary-connected sum is encoded in the combinatorics of $\mathcal{G}$. Eventually, no lateral 2-face of $\mathcal{D}^{(\ell)}_{ab}$ will be left free (for any a and b in the graph) and the only contributions to the boundary of $\mathcal{D}'$ will come from $s_a \setminus q_a$, $s_b \setminus q_b$ and Σ_{ab} (for any a and b). Its spine can be identified by noticing that each solid torus $\mathcal{D}^{(\ell)}_{ab}$ can be collapsed along ℓ_{ab} onto a S^1 homeomorphic to the boundary of o_{ab}. Thus, the spine of $\mathcal{D}'$ can be constructed by gluing the spines of each building block.[21] ∎

Let us turn our attention to draw of a set of γ-curves on the boundary of $\mathcal{D}'$. Four sectors of compression discs can be built in each $\mathcal{D}^{(\ell)}_{ab}$ intersecting the central surface on Σ_{ab} as well as on $s_a \setminus q_a$ and $s_b \setminus q_b$ (see Figure 15 (a)). The resulting four arcs of γ-curves correspond to arcs of four circles coplanar to the axis of revolution of the torus boundary of each $\mathcal{D}^{(\ell)}_{ab}$. Each arc starts from one of the sides of s_a (determined by a color $i \neq 0$), proceed along Σ_{ab} (therefore parallel to a 0-colored line of $\mathcal{G}$), and end on the side of s_b carrying the same color as the side they started from, as depicted in Figure 15. Here, each arc will connect to another one coming from a neighboring building block of $\mathcal{D}'$. Thanks to the combinatorics of $\mathcal{G}$, inherited by the building block of $\mathcal{D}'$, the composition of a γ-curve through the union of such arcs will go on according to the $\{0i\}$-colored cycles in the graph and close after as many iteration as the half of the length of the $\{0i\}$-cycle. Therefore, from each 0-colored tetrahedron τ_{ab}, four γ-curves depart each going around a boundary triangle. We remark here that this procedure gives us redundant γ-curves.

We conclude this section by simply performing the following identifications with respect to our Definition 4.1:

$$H_{23} = \mathcal{D}', \quad H_{12} = \mathcal{Q}', \quad H_{13} = \mathcal{R}'.$$

4.5. Four-dimensional handlebodies

Let us briefly comment on the four-dimensional pieces X_1, X_2, and X_3 we obtained with our prescription. As we discussed at the beginning of Section 4, theorem 4.2 implies that there is a unique cap-off of $\mathcal{D}' \cup \mathcal{Q}' \cup \mathcal{R}'$, i.e., there is a unique way of defining X_1, X_2, and X_3 using only 3- and 4-handles such that the pairwise unions $\mathcal{D}' \cup \mathcal{Q}'$, $\mathcal{D}' \cup \mathcal{R}'$ and $\mathcal{Q}' \cup \mathcal{R}'$, are the boundaries of X_1, X_2, and X_3. Due to the

[21] We recall that the boundary of each o_{ab} face consists of four sides carrying colors $i \neq 0$.

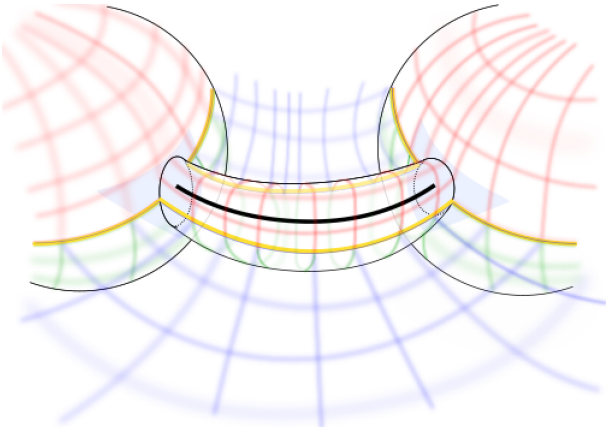

Figure 16. We illustrate how we connect the isolated dual of 4-bubbles via the carving operation explained in Section 4.4. For simplicity, the figure is an analogue in lower three dimensions rather than four. Two S^2's on the right and on the left represent $K(B^0_a)$ and $K(B^0_b)$ and they are connected via a tubular neighborhood of ℓ (here represented with a solid black line). Part of H_{12} is shown as a red surface, H_{13} in green, and H_{23} in blue. Part of the central surface to be is depicted as lines in yellow. The three-dimensional space above the red and the blue surfaces is an analogue of X_2, the one below is X_3, whereas the tubular neighborhood ℓ and the spheres constitute X_1. The light blue triangles represent $\mathcal{Q}_{\sigma_a} \cup \mathcal{R}_{\sigma_a}$ and $\mathcal{Q}_{\sigma_b} \cup \mathcal{R}_{\sigma_b}$. (See Figure 14.)

symmetric nature of i-handles and $(d-i)$-handles in d dimensions, all X_1, X_2, and X_3 are guaranteed to be handlebodies. The statement, therefore, is equivalent to saying that there is a unique set of three handlebodies with the given boundaries. Nevertheless, one might wonder whether, given a triangulation, these handlebodies actually reconstruct the PL-manifold or not. In fact, embedding $\mathcal{D}'$, $\mathcal{Q}'$ and $\mathcal{R}'$ in the triangulation as we illustrated above provides us with three four-dimensional submanifolds $\bar{X}_1$, $\bar{X}_2$ and $\bar{X}_3$ (see Figure 16 for a schematic representation of such an embedding). These manifolds share the same boundaries as X_1, X_2, and X_3 but they are a priori different. If that were the case, $\bar{X}_1$, $\bar{X}_2$ and $\bar{X}_3$ would automatically not be handlebodies due to the aforementioned uniqueness. In order to clarify this point we look for the spines of $\bar{X}_1$, $\bar{X}_2$ and $\bar{X}_3$.

Corollary 4.6. *Given a colored triangulation $\mathcal{T}$ of a manifold M, dual to a colored graph $\mathcal{G}$, and a choice of a jacket for its $\hat{0}$-bubbles, $\mathcal{J}(\mathcal{B}^{\hat{0}}_a)$, Construction 4.4 defines a trisection of M.*

Proof. Since the three-dimensional handlebodies $\mathcal{Q}'$, $\mathcal{D}'$ and $\mathcal{R}'$ satisfy the hypothesis of Definition 4.1 by construction (i.e., they share the same boundary and their interiors are disjoint), we can focus on the four-dimensional submanifolds $\bar{X}_1$, $\bar{X}_2$

and $\bar{X}_3$. Their interior is disjoint by construction, therefore the only issue is to prove that they are handlebodies. $\bar{X}_1$ is bounded by $\mathcal{Q}' \cup \mathcal{R}'$. Its spine is easily found by collapsing $K(\mathcal{B}_a^{\hat{0}})$ to points[22] and keeping the connection encoded by 0-colored embedded lines. Therefore, $\bar{X}_1$ is a handlebody by construction. $\bar{X}_2$ is bounded by $\mathcal{Q}' \cup \mathcal{D}'$. Bearing in mind the linear map from a $\Delta^{(4)}$ to $\Delta^{(2)}$ as in Section 4.2 (see Figure 12), we notice that in every four-simplex, $\bar{X}_2$ can be retracted to an edge identified by the set of colors $\{1, 2\}$ via its endpoints: $v^{\hat{1}}$ and $v^{\hat{2}}$. The set of these edges therefore constitutes a spine of $\bar{X}_2$. Moreover, $\bar{X}_2$ is connected since its boundary $\partial\bar{X}_2$ is connected by construction. This is enough to prove that $\bar{X}_2$ is a handlebody too. The argument for $\bar{X}_3$ follows in complete analogy with the one for $\bar{X}_2$ upon replacing the set of colors $\{1, 2\}$ with $\{3, 4\}$ and the boundary $\partial\bar{X}_2 = \mathcal{Q}' \cup \mathcal{D}'$ with $\partial\bar{X}_3 = \mathcal{R}' \cup \mathcal{D}'$.

The uniqueness of the handlebodies with the given boundary implies $\bar{X}_1 = X_1$, $\bar{X}_2 = X_2$ and $\bar{X}_3 = X_3$. ∎

4.6. Central surface and trisection diagram

In this section, we discuss the trisection diagram encoded in what we illustrated in Section 4.

Let us slowly reveal the topological information somewhat deeply hidden in our construction. From our construction, in general, the genus of the central surface will not coincide with the trisection genus. In a rare case the genus of the central surface is equal to the trisection genus, one could imagine it being a very special type of triangulation and is suppressed in the statistical theory dictated by the tensor model. This is not necessarily a dramatic problem, provided that there is a clear understanding of α-, β- and γ-curves. This information of curves, however, is also not necessarily trivial to extract since we generate many copies of the same curve which, in principle, intersect other curves on the diagram differently and choosing one curve over the other corresponds to a different diagram with the same central surface.[23] Nevertheless, we are hopeful that future works might unentangle this information and overcome this ambiguity.

To start, we look at the genus of the central surface. Let us define the following graph $\widetilde{\mathcal{G}}$ derived from a colored graph $\mathcal{G}$. Starting from the original colored graph $\mathcal{G}$, we collapse all the $\hat{0}$-bubbles to points which will become the nodes of $\widetilde{\mathcal{G}}$. Then, we connect these nodes via the 0-colored lines of $\mathcal{G}$ encoding the same combinatorics

[22] For the moment we are only dealing with manifolds rather than pseudo-manifolds therefore this just represents the retraction of a topological ball to its center.

[23] Therefore, connected by a series of handle slides and by as many handle addition as handle cancellations.

of the original graph $\mathcal{G}$. Effectively, the 0-colored lines of $\mathcal{G}$ simply become the lines of $\widetilde{\mathcal{G}}$. Note that the number of connected components of a graph is preserved under this operation; if $\mathcal{G}$ is connected, $\widetilde{\mathcal{G}}$ is connected. The number of loops[24] of $\widetilde{\mathcal{G}}$ corresponds to the dimension of its first homology group and evaluates to

$$L = |\mathcal{E}| - |\mathcal{V}| + 1,$$

where $|\mathcal{E}|$ is the number of lines and $|\mathcal{V}|$ is the number of nodes of $\widetilde{\mathcal{G}}$. By construction, $|\mathcal{V}|$ corresponds to the number of different $\hat{0}$-bubbles which, in turn, is the number of vertices opposing to 0-colored tetrahedra. The number $|\mathcal{E}|$, on the other hand, corresponds to the number of 0-colored tetrahedra and evaluates to $p/2$ for a triangulation of p simplices.[25]

Proposition 4.7. *Construction 4.4 defines a trisection with a central surface Σ of genus g_c given by*

$$g_c = \sum_{a=1}^{|\mathcal{V}|} g_{\mathcal{J}(\mathcal{B}_a^{\hat{0}})} + L, \tag{4.1}$$

with $g_{\mathcal{J}(\mathcal{B}_a^{\hat{0}})}$ being the genus of the jacket $\mathcal{J}_{\{1,2\}\{3,4\}}$ of the bubble $\mathcal{B}_a^{\hat{0}}$.

Notice that g_c is invariant under the insertion of 4-dipoles in the 0-colored lines, while inserting a 4-dipole in a line of color $i \neq 0$ increases L, and therefore g_c, by one. In fact, as we show in the Appendix A, the elementary melon yields the genus-1 trisection diagram for S^4 and the insertion of a 4-dipole can be understood as the connected sum with the elementary melon at the level of the colored graph.

Let us look at the curves we have drawn on Σ. We remark that the genus g_c also corresponds to the number of independent α-, β- and γ-curves. The γ-curves are obtained as paths on Σ and composed by segments parallel to the lines of $\widetilde{\mathcal{G}}$, and segments crossing the boundaries between different s's, according to an associated color $i \neq 0$. The composition of these segments according to the combinatorics of $\mathcal{G}$ forces the γ curve to close in a loop (see Figure 15 (b)). This tells us that the γ-curves are isomorphic to embedded $\{0i\}$-cycles in $\mathcal{T}$. Note that by representing the graph $\mathcal{G}$ in stranded notation, these curves are literally drawn on the surface.[26]

[24] We refer here to the notion of loops of a graph that is commonly used in physics in the framework of Feynman diagrams, not to the graph theoretical notion of a line connecting a node to itself. What we refer to as loop is, in graph theory, sometimes referred to as independent cycles.

[25] Note that we consider only orientable manifolds and, therefore, the original graph $\mathcal{G}$ is bipartite.

[26] Note that every vertex of $\mathcal{G}$ corresponds to a square in the surface dual to $\mathcal{J}(\mathcal{B}^{\hat{0}})$ and the 0-colored embedded lines are interpreted as handles. Therefore, the $\{0i\}$-strand is really isomorphic to one of the γ-curves.

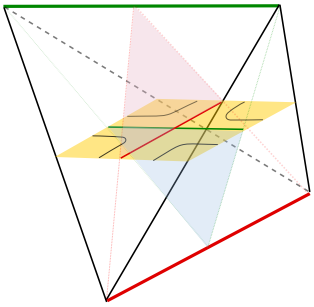

Figure 17. This sub-3-simplex is an element in the triangulation dual to a $\hat{0}$-bubble. We can identify α-curve (red line) and β-curve (green line) on the central surface (yellow square) by projecting the edges (red and green) of the sub-3-simplex sitting opposite to the central surface down to the central surface itself. These edges become part of the spine of the corresponding three-dimensional handlebodies. Part of compression discs are shown in pink (light blue) which is bounded by an α-curve (β-curve). We highlight the matrix model dual to a jacket $\mathcal{J}(\mathcal{B}^{\hat{0}})$. The yellow square which is part of central surface is nothing but the quadrangulation dual to a jacket $\mathcal{J}(\mathcal{B}^{\hat{0}})$. We illustrate that these trisection curves (α-curve in red and β-curve in green) coincide with drawing the strands of the original graph directly on the quadrangulation of the central surface.

Similarly, given a chosen jacket $\mathcal{J}_{\{i,j\}\{k,l\}}$, the (i, j)- and (k, l)-strands of $\mathcal{G}$ give the α- and β-curves (see Figure 17). Furthermore, we shall add one α- and one β-curve for every line $\widetilde{\mathcal{G}}$. These last additions correspond to the attaching curves of the Heegaard splitting of $S^1 \times S^2$ in the genus-1 trisection diagram of S^4 (see Section 4.1).

As we stated above, not all these curves are independent. Each of them is a viable attaching curve, but not all of them should be considered at the same time. For the α-curves (and similarly for the β-curves), we can constrain slightly more; the independent ones should be chosen to be $g_{\mathcal{J}(\mathcal{B}^{\hat{0}}_a)}$-many in each realization of a $\hat{0}$-bubble plus L-many among the extra ones we draw around the now embedded lines of $\widetilde{\mathcal{G}}$ (up to Heegaard moves). Remember that attaching curves of a graph are defined by the condition that cutting along them we obtain a connected punctured sphere (see Figure 5). L is by construction the maximal number of lines we can cut before disconnecting the graph $\widetilde{\mathcal{G}}$. Once these first L curves are cut, we can proceed identifying the rest of the α-curves given by each of the $|\mathcal{V}|$-many $\hat{0}$-bubbles through $\mathcal{J}(\mathcal{B}^{\hat{0}})$.

So far, we have treated color 0 to be special, however, of course that is an arbitrary choice for an easy illustration, and any other color choice will suffice. Hence, there are 15 possible trisections (up to handle slides) that can be generated with our construction (5 choices of 4-bubbles and 3 choices of jackets per each choice of 4-bubble).

A final remark is in order. If we compare our results with the one presented in [29], the genus of the central surface we obtain is obviously higher and less indicative of the

topological invariant. A more striking difference is that we have an extra combinatorial contribution. By construction, and due to the properties of the graphs considered, the result presented in [29] is only affected by the Heegaard splitting of an embedded 3-manifolds, in particular, the Heegaard splitting of the link of a vertex. Moreover, for a closed compact 4-manifold M, such link is always PL-homeomorphic to S^3. Thus, we can understand the trisection genus of a manifold M, which is a smooth invariant, as a lower bound for the possible Heegaard splittings of embedded spheres induced by colored triangulations of M. In our construction, however, an extra contribution to the genus of the central surface is produced in the form of L in equation (4.1). One may wonder whether this contribution is actually necessary or just an artifact of our construction of trisections. In other words, if the relevant topological information could indeed be rephrased in terms of Heegaard splittings of embedded 3-manifolds, it might be enough to consider the connected sum of the realizations of 4-bubbles, without systematically stabilizing the trisection with L extra of 1-handles.

4.7. Singular manifolds

What we have discussed so far strictly applies only to manifolds, i.e., to graphs where all $\hat{i}$-bubbles are dual to PL-spheres. Nevertheless, colored graphs generated by a colored tensor model of form (2.1) encode pseudo-manifolds as well. It is natural to wonder whether our construction might encode any sensible topological information for such wider class of graphs. In [29] such an extension has been made clear starting from crystallization graphs. We will follow similar steps in order to extend the same construction beyond graphs encoding closed compact manifolds.

Let us restrict to the case of $\widetilde{M} = K(\mathcal{G})$ being singular manifolds. Then, all the $\hat{i}$-bubbles are dual to PL-manifolds and the singularity is only around vertices in $\mathcal{T}$ (rather then higher-dimensional simplices). One can obtain a compact manifold M out of $\widetilde{M}$ by simply removing open neighborhoods of the singular vertices in $\mathcal{T}$. The number of connected components of ∂M will increase by the number of singular vertices with respect to the number of connected components of $\partial\widetilde{M}$. Conversely, one can obtain a singular manifold by coning all the boundary components of a manifold with (non-spherical) boundary. If $\mathcal{G}$ is a closed graph, then the above correspondence is a bijection between the set of manifolds with non-spherical boundary components and singular manifolds.

Although such bijection allows us to work with manifolds in a larger class of graphs, the definition of trisections as formulated in Definition 4.1 only applies to closed manifolds. Hence, we shall extend it to include boundary components in order to connect with our combinatorial construction. Following [29], we define a *B-trisection* by allowing one of the four-dimensional submanifolds not to be a handlebody.

Definition 4.8. Let M be an orientable, connected 4-manifold with n boundary components $\partial M_1, \ldots, \partial M_n$. A B-trisection of M is a collection of three submanifolds $X_1, X_2, X_3 \subset M$ such that:

- each X_1 and X_2 are four-dimensional handlebodies of genus g_1 and g_2, respectively,
- X_1 is a compression body with topology $\natural_{r=1}^{n}(\partial M_r \times [0,1]) \bigcup_{s=0}^{g_1} \mathrm{h}_s$, where h_s being 1-handles,
- X_i's have pairwise disjoint interiors $\partial X_i \supset (X_i \cap X_j) \subset \partial X_j$ and $M = \bigcup_i X_i$,
- the intersections $X_i \cap X_j = H_{ij}$ are three-dimensional handlebodies,
- the intersection of all the four-dimensional handlebodies $X_1 \cap X_2 \cap X_3$ is a closed connected surface Σ called *central surface*.

Let us further denote with $G_s^{(0)}$ the set of connected 5-colored graphs with only one $\widehat{0}$-bubble and with all $\hat{\imath}$-bubbles dual to topological spheres, and let us denote with $\overline{G}_s^{(0)}$ the set of connected 5-colored graphs whose only non-spherical bubbles are $\widehat{0}$-bubbles (but we do not restrict the number of such bubbles). Obviously, an element in $\overline{G}_s^{(0)}$ describes a manifold that can be decomposed into the connected sum of realizations of elements of $G_s^{(0)}$. The connected sum, in this case, can be performed at the level of two graphs $\mathcal{G}_1$ and $\mathcal{G}_2$ by cutting a 0-colored line in each graph and connecting the open lines of $\mathcal{G}_1$ to the open lines of $\mathcal{G}_2$. The construction of trisections we illustrated in the previous sections can be straightforwardly applied to graphs in $\overline{G}_s^{(0)}$ and it is easy to see that the outcome satisfies the conditions in Definition 4.8. In this regard, the result is the simplest generalization of the result presented in [29]. A more complicated extension would require the inclusion of singular vertices defined by different color sets; we leave such study for future works.

5. Conclusions

We have formulated trisections in the colored triangulations encoded in colored tensor models, restricting to the ones which are realized by manifolds (as opposed to pseudo-manifolds). We utilized the embedding of colored tensor model graphs in their dual triangulations to facilitate our construction of trisections. Generally speaking, the genus of the central surface of the trisection, given a colored tensor model graph, is higher as the graph is bigger (i.e., the number of nodes is larger). Therefore, statistically speaking, it is unlikely to obtain the trisection genus (which is a topological invariant) of the corresponding manifold of a given colored tensor model graph. Nevertheless, it would be interesting to investigate whether the construction of trisections might lead to new insights on the organization of the partition function of colored tensor models.

With the Gurau degree classifying tensor model graphs, we can achieve a large N limit, where we only select the dominating melonic graphs which are a subclass of spheres. Melons in the continuum limit have been shown to behave like branched polymers with Hausdorff dimension 2 and the spectral dimension $4/3$ [20, 65]. Reflecting and motivated by the quantum gravity context, we dream of a possibility of finding a new parameter for colored tensor model that can classify the graphs in a new large N limit, which may then give some new critical behavior. There have been works in this direction [13, 15, 16, 18], where the authors studied how to achieve different universality classes than the melonic branched polymer (tree). In [83], given random discrete spaces obtained by gluing families of polytopes together in all possible ways, with a systematic study of different building blocks, the author achieved the right scalings for the associated tensor models to have a well-behaved $1/N$ expansion. So far, one could achieve in addition to the tree-like phase, a two-dimensional quantum gravity planar phase, and a phase transition between them which may be interpreted as a proliferation of baby universes [84]. In [1,28,40,41,106], they have defined a new large N expansion parameter, based on an enhanced large N scaling of the coupling constants. These are called generalized melons, however, this class of graphs is not yet completely classified, and it is not proven yet what kind of universality class they belong to in the continuum limit, but strong hints point toward branched polymers. In the present case, knowing that in rank 3, the realisation of a jacket is identified to be a Heegaard surface, and knowing that jackets govern the Gurau degree which is responsible for the melonic large N limit, it is tempting to delve further into the possibility of finding a specific parameter for rank-4 colored tensor model based on trisections which may classify the graphs in the large N limit. Our next hope is to explore possibilities around trisections to find such a parameter.

Looking at the structure of equation (4.1) and its properties under d-dipoles insertion/contraction we expect melons to persist in dominating the large N. Nevertheless, a different parameter of topological origin might be induced by the above construction. An example is the intersection form, which we plan to investigate in the future following [39]. Hopefully investigations in this direction might shed some light on the path integral of tensor models beyond the leading order in the large N.

A. Examples

In this section, we present some particularly simple examples of trisections constructed via our procedure. We also show how to relate the diagrams obtained through our formulation to actual trisection diagrams for the manifolds we consider. In general, our prescription generates an excess amount of α-, β-, and γ-curves. One would like to get rid of the excess so that for each set of curves, we obtain a homotopically

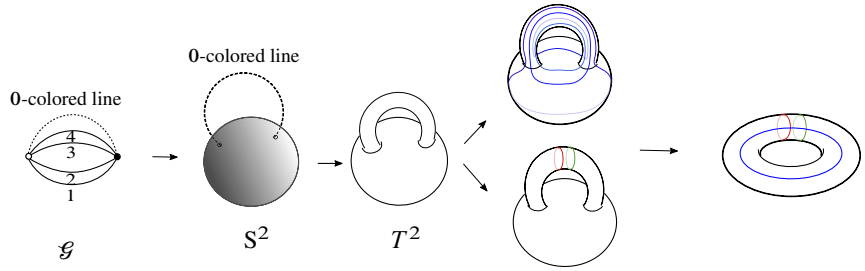

Figure 18. Construction of a trisection diagram for S^4 starting from the elementary melon. The first three picture represent, from left to right, the colored graph, the Heegaard surface for the $\widehat{0}$-bubble, the torus obtained after carving a regular neighborhood of the 0-colored line. The fourth picture represents the γ-curves (on top) and the α- and β-curves one has to add by hand when stabilizing (on the bottom). The last picture represents the trisection diagram after the redundant γ-curves have been removed.

independent system. This will give a trisection diagram for the corresponding manifold for the colored tensor model graph under consideration. We comment on how to retrieve such independent systems on some examples.

The first graph we consider is the elementary melon, shown in Figure 18. This is the simplest graph we can draw and consists of only two nodes sharing all the lines. In fact, this is the graph corresponding to the crystallization of S^4. Due to the melonic nature of this graph, we know that all the jackets are spheres. Also, all the bubbles are melons as well. Therefore, it affords the perfect playground to understand advantages and disadvantages of the procedure presented in Section 4.4, as well as the differences with the work presented in [29]. As we know from the smooth case, the trisection genus of S^4 is $g_{S^4} = 0$. Following [29], the trisection genus can be directly computed through the jackets of a bubble $\mathcal{B}^{\hat{i}}$. Since all the bubbles are melons as well, their jackets have indeed genus $g_{\mathcal{J}} = 0$. Following our construction, we add an extra handle to the central surface tracing the i-colored line. As shown in Figure 18, this step comes with the introduction of attaching curves. Following the conventions of the main text, we add one α-curve and one β-curve parallel to each other (red and green in the figure), and four γ-curves (in blue). Since these curves should represent the boundary of compression discs for handlebodies, homotopically equivalent curves are to be identified. Therefore, we collapse the four γ-curves to the same one. As anticipated, the result is one of the genus-1 trisection diagrams for S^4 that can be used to stabilize a trisection diagram.

Figure 18 does not take into account the attaching curves coming from the jacket. This can be justified by the fact that the jacket is spherical and, therefore, every closed curve on it is homotopically trivial. Nevertheless, one may wonder whether retaining such curves until the end of the construction gives rise to further possibilities. In this

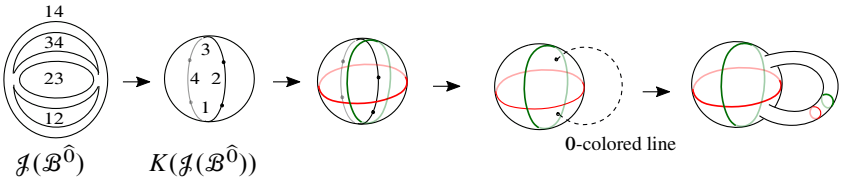

Figure 19. Alternative construction of a central surface for S^4 starting from the elementary melon. We repeat the same construction as in Figure 18, however this time we highlight the α- and β-curves induced by the jacket choice. From the rightmost picture, we see these curves are either trivial or isotopic to the curves induced by the stabilization.

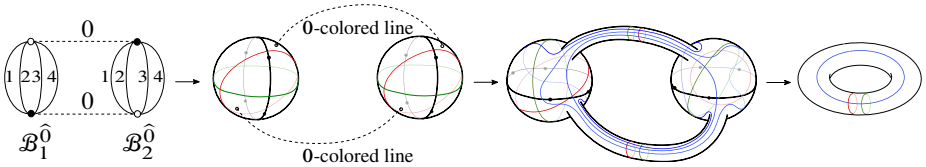

Figure 20. Construction of a trisection diagram for S^4 starting from the pillow diagram. We consider a melonic insertion in the 0-colored line of the elementary melon. When splitting the two connected components of $\mathcal{B}^{\hat{0}}$ we get two 2-spheres connected by two 0-colored lines as shown in the second picture from the left. The third picture from the left represents the surface obtained after the carving operation with all the α-, β- and γ-curves produced by the procedure. In this case, the central surface obtained after removing the redundant curves coincides with the one in Figure 18.

example, we see easily from Figure 19 that the curves obtained by the spherical jacket of $\mathcal{B}^{\hat{0}}$ end up being either redundant (i.e., homotopic to another curve of the same set) or trivial (i.e., homotopic to a point). The independent curves resulting from Figure 19 coincide with the red and green curves in the last diagram of Figure 18. We remind the reader that the number of curves in each set has to be equal to the genus of the surface for the diagram to be a trisection diagram.

Another interesting example is given by the pillow diagram. This diagram is melonic and results from inserting a d-dipole into the elementary melon. Holding on to our choice of having 0 as the special color, we have two possible ways of inserting such a dipole: inserting the dipole in a 0-colored line or inserting it in a i-colored line for $i \neq 0$. As discussed in Section 4.6, such choices lead to different results. In Figure 20, one can see how inserting a dipole in a 0-colored leads to the same diagram we found before. Figure 21, on the other hand, shows the construction of a trisection diagram with genus $g = 2$, due to the insertion of a 4-dipole in an i-colored line of the elementary melon, for $i \neq 0$. Here, we observe that, up to isotopy, we can obtain five different trisection diagrams of genus-2 for the sphere S^4 that, again, are obtained by considering only pairs of homotopically independent curves in each set. Nevertheless,

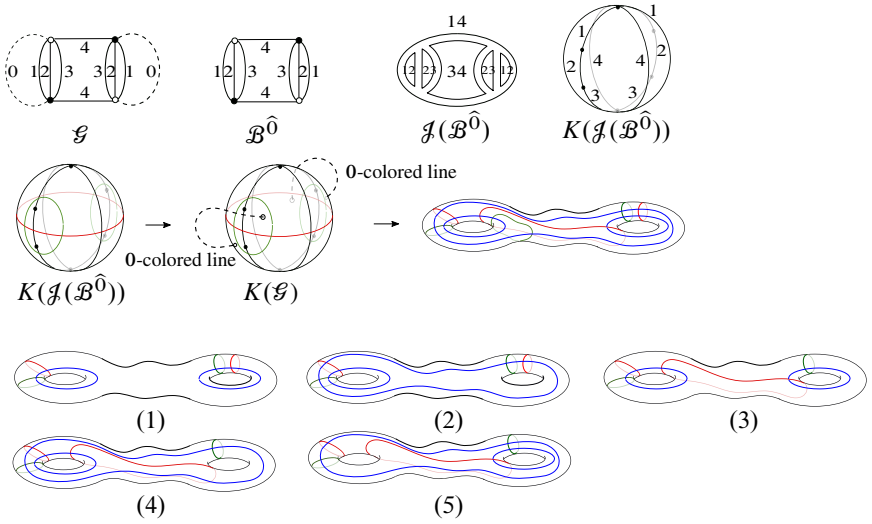

Figure 21. We consider a melonic insertion in the i-colored line of the elementary melon. In this case, we obtain a genus-2 central surface. In the top line of figures we obtain the Heegaard surface for $\mathcal{B}^{\widehat{0}}$ and show the corresponding jacket. In the second line, we insert the 0-colored lines and obtain the central surface with all the (redundant) curves. Finally, we display the five possible choices of trisection diagrams.

one may notice that, as expected, all these diagrams are connected by an appropriate handle slide. In fact, (2) is obtained starting from (1) by a handle slide of one of the blue curves, (3) is obtained from (1) by a handle slide of one of the red curves, while (4) and (5) are different handle slides of a red curve in (2). Note that the handle slides of the red curves relate a curve coming from the quadrangulation dual to the jacket with one of those added through stabilization.

Finally, let us look at the graph shown in Figure 22. Although not melonic, this diagram still corresponds to a sphere. Out of the fifteen possible choices for constructing a central surface, we look at the less trivial one. Removing either the color 3 or the color 4, leads to a surface of genus-2. On the contrary, removing the color 0 (or equivalently the colors 1 or 2), leads to a necklace-like bubble. Such bubbles have one jacket which is not spherical, but rather dual to a torus. This is the choice we consider in the example shown in Figure 22. Let us note how, already for such a simple graph, we obtain a huge proliferation of redundant attaching curves, leading to different trisection diagrams. In particular, looking at the different ways we have to choose the attaching curves in this example, we obtain sixteen possible trisection diagrams of genus-3 for the sphere S^4, all out of a single combinatorial choice (out of fifteen possible choices).

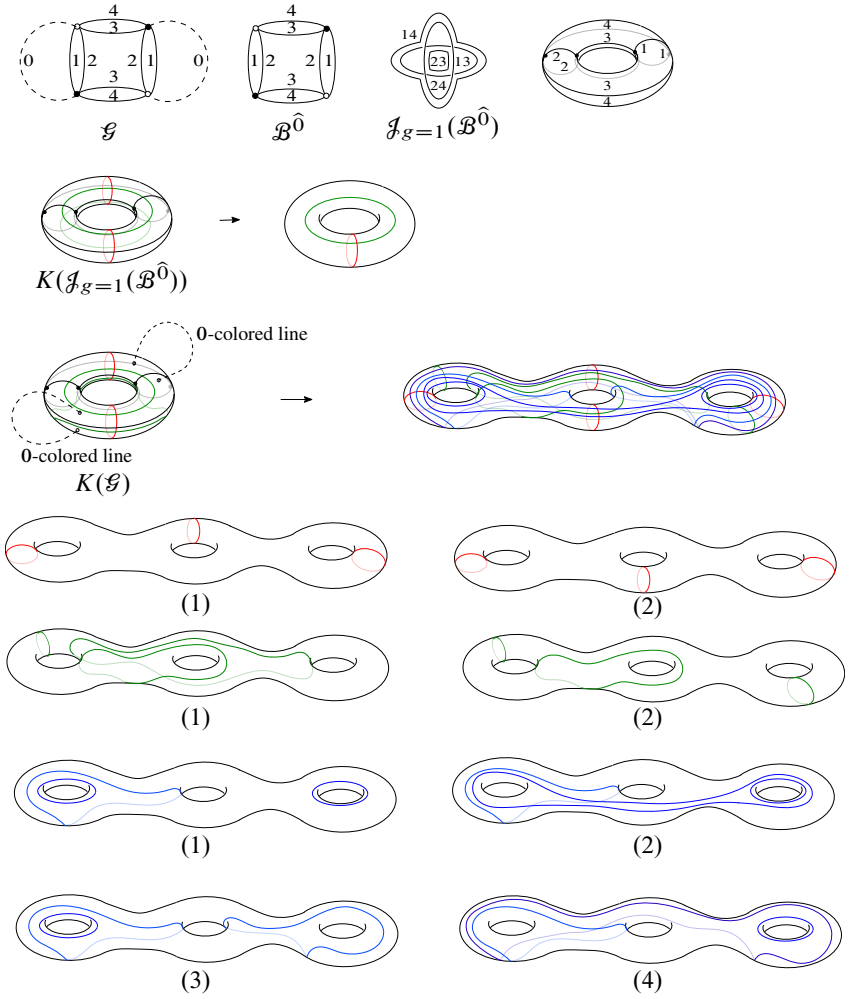

Figure 22. Example of trisection diagrams for S^4 obtained by the necklace diagram $\mathcal{G}$. We choose the only toroidal jacket of $\mathcal{B}^{\hat{0}}$. In the second line, we show how this jacket leads to the genus-1 Heegaard diagram for S^3. The third line of pictures shows the introduction of the 0-colored line and the central surface comprised of all the redundant information. Then, we display the possible choices of compatible curves for each set of attaching curves.

To understand this, we show in Figure 22 the viable choices for each of the three sets of curves. We remind the reader that cutting along the attaching curves we are not allowed to disconnect the surface; this would mean that we are either cutting along a curve that does not define a 1-handle or that is not homotopically independent of those already considered. For example, considering the red curves, we only have two choices since the two meridian curves for the central hole cannot be chosen at the same time (they are indeed connected by two handle slides). A similar consideration

takes place for the set of green curves. For example, considering diagram (1) for green curves and substituting the meridian curve on the left for the meridian curve on the rightmost handle (appearing in diagram (2) for the green curves) would split the surface. This is precisely because the resulting curves would not be homotopically independent. In the same way, a close inspection on the blue curves leave us with only four possible choices. As a result, one can obtain $2 \times 2 \times 4 = 16$ possible trisection diagrams of genus-3 for the same manifold.

Acknowledgments. We would like to thank Andrew Lobb for giving us a lecture on Morse theory, for supervising us on a study on trisections and for other discussions while he was visiting OIST as an excellence chair in the OIST Math Visitor Program. We would also like to thank David O'Connell for leading study sessions on trisections with us. Furthermore, we thank Maria Rita Casali and Paola Cristofori as well as Razvan Gurau for checking our formulation and the manuscript.

References

[1] T. Azeyanagi, F. Ferrari, P. Gregori, L. Leduc, and G. Valette, More on the new large D limit of matrix models. *Ann. Physics* **393** (2018), 308–326 Zbl 1390.81287 MR 3805424

[2] P. Bandieri and C. Gagliardi, Generating all orientable n-manifolds from $(n-1)$-complexes. *Rend. Circ. Mat. Palermo (2)* **31** (1982), no. 2, 233–246 Zbl 0492.57006 MR 670398

[3] M. Bell, J. Hass, J. H. Rubinstein, and S. Tillmann, Computing trisections of 4-manifolds. *Proc. Natl. Acad. Sci. USA* **115** (2018), no. 43, 10901–10907 Zbl 1420.57057 MR 3871794

[4] J. Ben Geloun, Two- and four-loop β-functions of rank-4 renormalizable tensor field theories. *Classical Quantum Gravity* **29** (2012), no. 23, article no. 235011 Zbl 1258.83033 MR 3002873

[5] J. Ben Geloun, Renormalizable models in rank $d \geq 2$ tensorial group field theory. *Comm. Math. Phys.* **332** (2014), no. 1, 117–188 Zbl 1300.83043 MR 3253701

[6] J. Ben Geloun and T. A. Koslowski, Nontrivial UV behavior of rank-4 tensor field models for quantum gravity. 2016, arXiv:1606.04044

[7] J. Ben Geloun, T. A. Koslowski, D. Oriti, and A. D. Pereira, Functional renormalization group analysis of rank-3 tensorial group field theory: the full quartic invariant truncation. *Phys. Rev. D* **97** (2018), no. 12, article no. 126018 MR 3893706

[8] J. Ben Geloun, T. Krajewski, J. Magnen, and V. Rivasseau, Linearized group field theory and power-counting theorems. *Classical Quantum Gravity* **27** (2010), no. 15, article no. 155012 Zbl 1195.81093 MR 2659247

[9] J. Ben Geloun, R. Martini, and D. Oriti, Functional renormalization group analysis of tensorial group field theories on $\mathbb{R}^3$. *Europhys. Lett.* **112** (2015), no. 3, article no. 31001 MR 3661338

[10] J. Ben Geloun, R. Martini, and D. Oriti, Functional renormalization group analysis of tensorial group field theories on $\mathbb{R}^d$. *Phys. Rev. D* **94** (2016), no. 2, article no. 024017 MR 3661338

[11] J. Ben Geloun and V. Rivasseau, A renormalizable 4-dimensional tensor field theory. *Comm. Math. Phys.* **318** (2013), no. 1, 69–109 Zbl 1261.83016 MR 3017064

[12] J. Ben Geloun and R. Toriumi, Parametric representation of rank d tensorial group field theory: Abelian models with kinetic term $\sum_s |p_s| + \mu$. *J. Math. Phys.* **56** (2015), no. 9, article no. 093503 Zbl 1322.83011 MR 3396221

[13] J. Ben Geloun and R. Toriumi, Renormalizable enhanced tensor field theory: the quartic melonic case. *J. Math. Phys.* **59** (2018), no. 11, article no. 112303 Zbl 1408.83024 MR 3880589

[14] D. Benedetti, J. Ben Geloun, and D. Oriti, Functional renormalisation group approach for tensorial group field theory: a rank-3 model. *J. High Energy Phys.* **2015** (2015), no. 3, article no. 084 Zbl 1388.83088 MR 3340520

[15] V. Bonzom, New $1/N$ expansions in random tensor models. *J. High Energy Phys.* **2013** (2013), no. 6, article no. 062 Zbl 1342.83053 MR 3083348

[16] V. Bonzom, Large N limits in tensor models: towards more universality classes of colored triangulations in dimension $d \geq 2$. *SIGMA Symmetry Integrability Geom. Methods Appl.* **12** (2016), article no. 073 Zbl 1343.05059 MR 3528381

[17] V. Bonzom and S. Dartois, Blobbed topological recursion for the quartic melonic tensor model. *J. Phys. A* **51** (2018), no. 32, article no. 325201 Zbl 1400.81159 MR 3829394

[18] V. Bonzom, T. Delepouve, and V. Rivasseau, Enhancing non-melonic triangulations: a tensor model mixing melonic and planar maps. *Nuclear Phys. B* **895** (2015), 161–191 Zbl 1329.81258 MR 3341951

[19] V. Bonzom and N. Dub, Blobbed topological recursion for correlation functions in tensor models. 2020, arXiv:2011.09399

[20] V. Bonzom, R. Gurau, A. Riello, and V. Rivasseau, Critical behavior of colored tensor models in the large N limit. *Nuclear Phys. B* **853** (2011), no. 1, 174–195 Zbl 1229.81222 MR 2831765

[21] V. Bonzom, R. Gurau, and M. Smerlak, Universality in p-spin glasses with correlated disorder. *J. Stat. Mech. Theory Exp.* **2013** (2013), no. 2, article no. L02003 Zbl 1456.82906 MR 3041899

[22] S. Carrozza, *Tensorial methods and renormalization in group field theories*. Springer Theses, Springer, Cham, 2014 Zbl 1338.81004 MR 3288079

[23] S. Carrozza, Discrete renormalization group for SU(2) tensorial group field theory. *Ann. Inst. Henri Poincaré D* **2** (2015), no. 1, 49–112 Zbl 1319.81068 MR 3336263

[24] S. Carrozza, Group field theory in dimension $4 - \varepsilon$. *Phys. Rev. D* **91** (2015), no. 6, article no. 065023 Zbl 1319.81068 MR 3415336

[25] S. Carrozza, Flowing in group field theory space: a review. *SIGMA Symmetry Integrability Geom. Methods Appl.* **12** (2016), article no. 070 Zbl 1343.81177 MR 3522313

[26] S. Carrozza, D. Oriti, and V. Rivasseau, Renormalization of a SU(2) tensorial group field theory in three dimensions. *Comm. Math. Phys.* **330** (2014), no. 2, 581–637 Zbl 1300.83023 MR 3223482

[27] S. Carrozza, D. Oriti, and V. Rivasseau, Renormalization of tensorial group field theories: Abelian U(1) models in four dimensions. *Comm. Math. Phys.* **327** (2014), no. 2, 603–641 Zbl 1291.83102 MR 3183411

[28] S. Carrozza and A. Tanasă, O(N) random tensor models. *Lett. Math. Phys.* **106** (2016), no. 11, 1531–1559 Zbl 1362.83010 MR 3555413

[29] M. R. Casali and P. Cristofori, Gem-induced trisections of compact PL 4-manifolds. 2022, arXiv:1910.08777

[30] M. R. Casali, P. Cristofori, S. Dartois, and L. Grasselli, Topology in colored tensor models via crystallization theory. *J. Geom. Phys.* **129** (2018), 142–167 Zbl 1398.57034 MR 3789242

[31] S. Dartois, H. Erbin, and S. Mondal, Conformality of $1/N$ corrections in Sachdev–Ye–Kitaev-like models. *Phys. Rev. D* **100** (2019), no. 12, article no. 125005 MR 4050385

[32] S. Dartois, O. Evnin, L. Lionni, V. Rivasseau, and G. Valette, Melonic turbulence. *Comm. Math. Phys.* **374** (2020), no. 2, 1179–1228 Zbl 1436.81095 MR 4072238

[33] F. David, A. Kupiainen, R. Rhodes, and V. Vargas, Liouville quantum gravity on the Riemann sphere. *Comm. Math. Phys.* **342** (2016), no. 3, 869–907 Zbl 1336.83042 MR 3465434

[34] N. Delporte and V. Rivasseau, The tensor track V: Holographic tensors. *Proc. of Sci.* **318** (2018), article no. PoS(CORFU2017)218

[35] N. Delporte and V. Rivasseau, The tensor track VI: Field theory on random trees and SYK on random unicyclic graphs. *Proc. of Sci.* **376** (2020), article no. PoS(CORFU2019)207

[36] P. Di Francesco, P. Ginsparg, and J. Zinn-Justin, 2D gravity and random matrices. *Phys. Rep.* **254** (1995), no. 1–2, 1–133 MR 1320471

[37] M. Disertori, R. Gurau, J. Magnen, and V. Rivasseau, Vanishing of beta function of non-commutative Φ^4_4 theory to all orders. *Phys. Lett. B* **649** (2007), no. 1, 95–102 Zbl 1248.81253 MR 2308801

[38] A. Eichhorn and T. Koslowski, Flowing to the continuum limit in tensor models for quantum gravity. *Ann. Inst. Henri Poincaré D* **5** (2018), no. 2, 173–210 Zbl 1392.81191 MR 3813214

[39] P. Feller, M. Klug, T. Schirmer, and D. Zemke, Calculating the homology and intersection form of a 4-manifold from a trisection diagram. *Proc. Natl. Acad. Sci. USA* **115** (2018), no. 43, 10869–10874 Zbl 1421.57028 MR 3871789

[40] F. Ferrari, The large D limit of planar diagrams. *Ann. Inst. Henri Poincaré D* **6** (2019), no. 3, 427–448 Zbl 1431.83092 MR 4002672

[41] F. Ferrari, V. Rivasseau, and G. Valette, A new large N expansion for general matrix-tensor models. *Comm. Math. Phys.* **370** (2019), no. 2, 403–448 Zbl 1480.81107 MR 3994575

[42] M. Ferri and C. Gagliardi, Crystallisation moves. *Pacific J. Math.* **100** (1982), no. 1, 85–103 Zbl 0517.57003 MR 661442

[43] M. Ferri, C. Gagliardi, and L. Grasselli, A graph-theoretical representation of PL-manifolds – a survey on crystallizations. *Aequationes Math.* **31** (1986), no. 2–3, 121–141 Zbl 0623.57012 MR 867510

[44] C. Gagliardi, Extending the concept of genus to dimension n. *Proc. Amer. Math. Soc.* **81** (1981), no. 3, 473–481 Zbl 0467.57004 MR 597666

[45] D. Gay and R. Kirby, Trisecting 4-manifolds. *Geom. Topol.* **20** (2016), no. 6, 3097–3132 Zbl 1372.57033 MR 3590351

[46] H. Grosse, A. Sako, and R. Wulkenhaar, Exact solution of matricial Φ^3_2 quantum field theory. *Nuclear Phys. B* **925** (2017), 319–347 Zbl 1375.81170 MR 3730482

[47] H. Grosse, A. Sako, and R. Wulkenhaar, The Φ^3_4 and Φ^3_6 matricial QFT models have reflection positive two-point function. *Nuclear Phys. B* **926** (2018), 20–48 Zbl 1380.81193 MR 3760253

[48] H. Grosse and H. Steinacker, Renormalization of the noncommutative ϕ^3 model through the Kontsevich model. *Nuclear Phys. B* **746** (2006), no. 3, 202–226 Zbl 1178.81190 MR 2235178

[49] H. Grosse and R. Wulkenhaar, Renormalisation of ϕ^4-theory on noncommutative $\mathbb{R}^4$ in the matrix base. *Comm. Math. Phys.* **256** (2005), no. 2, 305–374 Zbl 1075.82005 MR 2160797

[50] H. Grosse and R. Wulkenhaar, Self-dual noncommutative ϕ^4-theory in four dimensions is a non-perturbatively solvable and non-trivial quantum field theory. *Comm. Math. Phys.* **329** (2014), no. 3, 1069–1130 Zbl 1305.81129 MR 3212880

[51] H. Grosse and R. Wulkenhaar, Solvable 4D noncommutative QFT: phase transitions and quest for reflection positivity. 2015, arXiv:1406.7755

[52] R. Gurau, Lost in translation: topological singularities in group field theory. *Classical Quantum Gravity* **27** (2010), no. 23, article no. 235023 Zbl 1205.83022 MR 2738259

[53] R. Gurau, The $1/N$ expansion of colored tensor models. *Ann. Henri Poincaré* **12** (2011), no. 5, 829–847 Zbl 1218.81088 MR 2802384

[54] R. Gurau, The $1/N$ expansion of colored tensor models in arbitrary dimension. *Europhys. Lett.* **95** (2011), no. 5, article no. 50004

[55] R. Gurau, Colored group field theory. *Comm. Math. Phys.* **304** (2011), no. 1, 69–93 Zbl 1214.81170 MR 2793930

[56] R. Gurau, A generalization of the Virasoro algebra to arbitrary dimensions. *Nuclear Phys. B* **852** (2011), no. 3, 592–614 Zbl 1229.81129 MR 2826235

[57] R. Gurau, The complete $1/N$ expansion of colored tensor models in arbitrary dimension. *Ann. Henri Poincaré* **13** (2012), no. 3, 399–423 Zbl 1245.81118 MR 2909101

[58] R. Gurau, The $1/N$ expansion of tensor models beyond perturbation theory. *Comm. Math. Phys.* **330** (2014), no. 3, 973–1019 Zbl 1297.81126 MR 3227505

[59] R. Gurau, Invitation to random tensors. *SIGMA Symmetry Integrability Geom. Methods Appl.* **12** (2016), article no. 094 Zbl 1346.83030 MR 3550395

[60] R. Gurau, The complete $1/N$ expansion of a SYK-like tensor model. *Nuclear Phys. B* **916** (2017), 386–401 Zbl 1356.81180 MR 3611412

[61] R. Gurau, *Random tensors*. Oxford University Press, Oxford, 2017 Zbl 1371.81007 MR 3616422

[62] R. Gurau, The $1/N$ expansion of tensor models with two symmetric tensors. *Comm. Math. Phys.* **360** (2018), no. 3, 985–1007 Zbl 1393.81026 MR 3803815

[63] R. Gurau and V. Rivasseau, The multiscale loop vertex expansion. *Ann. Henri Poincaré* **16** (2015), no. 8, 1869–1897 Zbl 1321.81046 MR 3369319

[64] R. Gurau and J. P. Ryan, Colored tensor models – a review. *SIGMA Symmetry Integrability Geom. Methods Appl.* **8** (2012), article no. 020 Zbl 1242.05094 MR 2942819

[65] R. Gurau and J. P. Ryan, Melons are branched polymers. *Ann. Henri Poincaré* **15** (2014), no. 11, 2085–2131 Zbl 1303.83012 MR 3268825

[66] R. G. Gurau and T. Krajewski, Analyticity results for the cumulants in a random matrix model. *Ann. Inst. Henri Poincaré D* **2** (2015), no. 2, 169–228 Zbl 1353.60009 MR 3354330

[67] D. Kartsaklis, S. Ramgoolam, and M. Sadrzadeh, Linguistic matrix theory. *Ann. Inst. Henri Poincaré D* **6** (2019), no. 3, 385–426 Zbl 1447.91125 MR 4002671

[68] I. R. Klebanov and G. Tarnopolsky, On large N limit of symmetric traceless tensor models. *J. High Energy Phys.* **2017** (2017), no. 10, article no. 037 Zbl 1383.81239 MR 3731176

[69] I. R. Klebanov and G. Tarnopolsky, Uncolored random tensors, melon diagrams, and the Sachdev–Ye–Kitaev models. *Phys. Rev. D* **95** (2017), no. 4, article no. 046004 MR 3783911

[70] M. Kontsevich, Intersection theory on the moduli space of curves and the matrix Airy function. *Comm. Math. Phys.* **147** (1992), no. 1, 1–23 Zbl 0756.35081 MR 1171758

[71] T. Krajewski and R. Toriumi, Exact renormalisation group equations and loop equations for tensor models. *SIGMA Symmetry Integrability Geom. Methods Appl.* **12** (2016), article no. 068 Zbl 1343.81179 MR 3522020

[72] T. Krajewski and R. Toriumi, Polchinski's exact renormalisation group for tensorial theories: Gaußian universality and power counting. *J. Phys. A* **49** (2016), no. 38, article no. 385401 Zbl 1348.81335 MR 3544748

[73] C. Krishnan and K. V. Pavan Kumar, Towards a finite-N hologram. *J. High Energy Phys.* **2017** (2017), no. 10, article no. 099 Zbl 1383.81240 MR 3731114

[74] C. Krishnan, K. V. Pavan Kumar, and S. Sanyal, Random matrices and holographic tensor models. *J. High Energy Phys.* **2017** (2017), no. 6, article no. 036 Zbl 1380.83260 MR 3678397

[75] C. Krishnan, S. Sanyal, and P. N. B. Subramanian, Quantum chaos and holographic tensor models. *J. High Energy Phys.* **2017** (2017), no. 3, article no. 056 Zbl 1377.83049 MR 3657641

[76] V. Lahoche, M. Ouerfelli, D. Ousmane Samary, and M. Tamaazousti, Field theoretical approach for signal detection in nearly continuous positive spectra II: Tensorial data. *Entropy* **23** (2021), no. 7, article no. 795 MR 4292174

[77] V. Lahoche and D. Ousmane Samary, Nonperturbative renormalization group beyond the melonic sector: the effective vertex expansion method for group fields theories. *Phys. Rev. D* **98** (2018), no. 12, article no. 126010 Zbl 1418.81056 MR 3974318

[78] V. Lahoche and D. Ousmane Samary, Ward identity violation for melonic T^4-truncation. *Nuclear Phys. B* **940** (2019), 190–213 Zbl 1409.83068

[79] V. Lahoche and D. Ousmane Samary, Pedagogical comments about nonperturbative Ward-constrained melonic renormalization group flow. *Phys. Rev. D* **101** (2020), no. 2, article no. 024001 Zbl 1435.81136 MR 4066467

[80] J. Le Gall, Uniqueness and universality of the Brownian map. *Ann. Probab.* **41** (2013), no. 4, 2880–2960 Zbl 1282.60014 MR 3112934

[81] J. Le Gall and G. Miermont, Scaling limits of random trees and planar maps. In *Probability and statistical physics in two and more dimensions*, pp. 155–211, American Mathematical Society, Providence, RI, 2012 Zbl 1321.05240 MR 3025391

[82] S. Lins, *Gems, computers and attractors for 3-manifolds*. Ser. Knots Everything 5, World Sci. Publ., River Edge, NJ, 1995 Zbl 0868.57002 MR 1370443

[83] L. Lionni, *Colored discrete spaces: higher dimensional combinatorial maps and quantum gravity*. Springer Theses, Springer, Cham, 2018 Zbl 1406.81007 MR 3822340

[84] L. Lionni and J. Thürigen, Multi-critical behaviour of 4-dimensional tensor models up to order 6. *Nuclear Phys. B* **941** (2019), 600–635 Zbl 1415.83007 MR 3922507

[85] J. Meier, T. Schirmer, and A. Zupan, Classification of trisections and the generalized property R conjecture. *Proc. Amer. Math. Soc.* **144** (2016), no. 11, 4983–4997 Zbl 1381.57018 MR 3544545

[86] G. Miermont, The Brownian map is the scaling limit of uniform random plane quadrangulations. *Acta Math.* **210** (2013), no. 2, 319–401 Zbl 1278.60124 MR 3070569

[87] J. Miller and S. Sheffield, Liouville quantum gravity and the Brownian map I: The QLE(8/3, 0) metric. *Invent. Math.* **219** (2020), no. 1, 75–152 Zbl 1437.83042 MR 4050102

[88] J. Miller and S. Sheffield, Liouville quantum gravity and the Brownian map II: Geodesics and continuity of the embedding. *Ann. Probab.* **49** (2021), no. 6, 2732–2829 Zbl 1478.60045 MR 4348679

[89] J. Miller and S. Sheffield, Liouville quantum gravity and the Brownian map III: The conformal structure is determined. *Probab. Theory Related Fields* **179** (2021), no. 3–4, 1183–1211 Zbl 1478.60044 MR 4242633

[90] J. M. Montesinos, Heegaard diagrams for closed 4-manifolds. In *Geometric topology (Proc. Georgia Topology Conf., Athens, Ga., 1977)*, pp. 219–237, Academic Press, New York, 1979 Zbl 479.57007 MR 537732

[91] M. Nakahara, *Geometry, topology and physics*. 2nd edn., Grad. Stud. Ser. Phys., Institute of Physics, Bristol, 2003 Zbl 1090.53001 MR 2001829

[92] P. Narayan and J. Yoon, SYK-like tensor models on the lattice. *J. High Energy Phys.* **2017** (2017), no. 8, article no. 083 Zbl 1381.81091 MR 3697399

[93] C. Peng, Vector models and generalized SYK models. *J. High Energy Phys.* **2017** (2017), no. 5, article no. 129 Zbl 1380.81249 MR 3662802

[94] C. Peng, M. Spradlin, and A. Volovich, A supersymmetric SYK-like tensor model. *J. High Energy Phys.* **2017** (2017), no. 5, article no. 062 Zbl 1380.81355 MR 3662869

[95] A. M. Polyakov, Quantum geometry of bosonic strings. *Phys. Lett. B* **103** (1981), no. 3, 207–210 MR 623209

[96] S. Ramgoolam and M. Sedlák, Quantum information processing and composite quantum fields. *J. High Energy Phys.* **2019** (2019), no. 1, article no. 170 Zbl 1409.81129 MR 3919325

[97] V. Rivasseau, The tensor track, III. *Fortschr. Phys.* **62** (2014), no. 2, 81–107 Zbl 1338.83085 MR 3164678

[98] V. Rivasseau, The tensor track, IV. *Proc. of Sci.* **263** (2016), article no. PoS(CORFU2015)106

[99] V. Rivasseau and F. Vignes-Tourneret, Non-commutative renormalization. In *Rigorous quantum field theory. A Festschrift for Jacques Bros*, pp. 271–281, Progr. Math. 251, Birkhäuser, Basel, 2007 Zbl 1166.81363 MR 2279223

[100] V. Rivasseau, F. Vignes-Tourneret, and R. Wulkenhaar, Renormalisation of noncommutative ϕ^4-theory by multi-scale analysis. *Comm. Math. Phys.* **262** (2006), no. 3, 565–594 Zbl 1109.81056 MR 2202303

[101] J. H. Rubinstein, One-sided Heegaard splittings of 3-manifolds. *Pacific J. Math.* **76** (1978), no. 1, 185–200 Zbl 0394.57013 MR 488064

[102] J. H. Rubinstein and S. Tillmann, Generalized trisections in all dimensions. *Proc. Natl. Acad. Sci. USA* **115** (2018), no. 43, 10908–10913 Zbl 1421.57032 MR 3871795

[103] J. P. Ryan, Tensor models and embedded Riemann surfaces. *Phys. Rev. D* **85** (2012), no. 9, article no. 024010

[104] J. Spreer and S. Tillmann, The trisection genus of standard simply connected PL 4-manifolds. In *34th International Symposium on Computational Geometry*, pp. 71.1–71.13, LIPIcs. Leibniz Int. Proc. Inform. 99, Schloss Dagstuhl – Leibniz Zentrum für Informatik, Wadern, 2018 Zbl 1471.57018 MR 3824315

[105] G. 't Hooft, A planar diagram theory for strong interactions. *Nuclear Phys. B* **72** (1974), no. 3, 461–473

[106] G. Valette, New limits for large N matrix and tensor models: large D, melons and applications. PhD thesis, Université Libre de Bruxelles, 2019, arXiv:1911.11574

[107] Z. Wang, Construction of 2-dimensional Grosse–Wulkenhaar model. *Proc. of Sci.* **155** (2012), article no. PoS(CORFU2011)057

[108] E. Witten, An SYK-like model without disorder. *J. Phys. A* **52** (2019), no. 47, article no. 474002 Zbl 07638025 MR 4028950

Communicated by Adrian Tanasă

Received 17 November 2021; revised 20 April 2022.

Riccardo Martini
Okinawa Institute of Science and Technology, Graduate University, 1919-1, Tancha, Onna, Kunigami District, 904-0495 Okinawa, Japan; riccardo.martini@oist.jp

Reiko Toriumi
Okinawa Institute of Science and Technology, Graduate University, 1919-1, Tancha, Onna, Kunigami District, 904-0495 Okinawa, Japan; reiko.toriumi@oist.jp